Energy & Environmental Science

Accepted Manuscript

ROYAL SOCIETY OF CHEMISTRY

www.rsc.org/ees

Earth-abundant inorganic electrocatalysts and their nanostructures for energy conversion applications

*Matthew S. Faber and Song Jin**

Department of Chemistry, University of Wisconsin–Madison, 1101 University Avenue, Madison, Wisconsin 53706, USA

*E-mail: jin@chem.wisc.edu

Abstract

Electrocatalysis plays a key role in the energy conversion processes central to several renewable energy technologies that have been developed to lessen our reliance on fossil fuels. However, the best electrocatalysts for these processes—which include the hydrogen evolution reaction (HER), the oxygen reduction reaction (ORR), and the redox reactions that enable regenerative liquid-junction photoelectrochemical solar cells—often contain scarce and expensive noble metals, substantially limiting the potential for these technologies to compete with fossil fuels. The considerable challenge is to develop robust electrocatalysts composed exclusively of low-cost, earth-abundant elements that exhibit activity comparable to that of the noble metals. In this review, we summarize recent progress in the development of such high-performance earth-abundant inorganic electrocatalysts (and nanostructures thereof), classifying these materials based on their elemental constituents. We then detail the most critical obstacles facing earth-abundant inorganic electrocatalysts and discuss various strategies for further improving their performance. Lastly, we offer our perspectives on the current directions of earth-abundant inorganic electrocatalyst development and suggest pathways toward achieving performance competitive with their noble metal-containing counterparts.

Broader context

Renewable energy technologies will necessarily grow in importance if we are to meet our future energy demands. The goal is for these environmentally-friendly, alternative sources of energy to become cost competitive with fossil fuels, reducing our reliance on such limited

resources. For this to happen, though, the precious noble metal (or noble metal-containing) electrocatalysts used in these renewable energy technologies should be replaced with low-cost, earth-abundant substitutes that exhibit comparable catalytic activity and long-term stability. In this review, we first provide a broad overview of electrocatalysis and its role in several important renewable energy technologies, including water splitting to generate hydrogen fuel, the reduction of oxygen in fuel cell devices, and the regenerative operation of photoelectrochemical solar cells. We then discuss the various classes of earth-abundant electrocatalysts presently under investigation, highlighting important advances, emerging trends in their development, and the challenges facing them, before finally offering our perspectives on how to most effectively advance the development of earth-abundant inorganic electrocatalysts.

Graphical Abstract

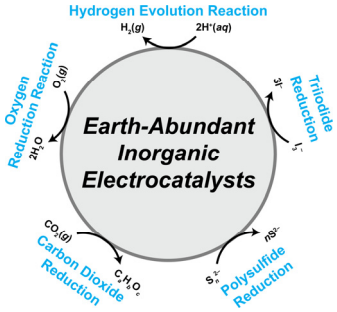

Graphical Abstract text

Various classes of earth-abundant inorganic electrocatalysts for energy conversion are surveyed and their recent and ongoing development is discussed.

1. Introduction

In recent decades, there has been a growing need to replace fossil fuels with environmentally-friendly, secure, and sustainable alternative sources of energy. Renewable energy technologies generally rely on harvesting and storing energy from our most readily exploitable and only truly limitless source: the Sun. The primary argument in favor of transitioning to renewable sources of energy is indeed quite compelling: with the amount of energy received from solar insolation vastly exceeding that consumed globally, capturing and utilizing a mere fraction could significantly offset or even obviate our need for fossil fuels.[1] Inspired by this highly attractive prospect, researchers have spent decades developing materials and devices capable of converting sunlight into electricity. Device designs ranging from completely solid-state single-crystalline photovoltaics[2] to liquid-junction photoelectrochemical solar cells[3] have been explored and shown to operate at varying (yet steadily improving) levels of solar light-to-electricity power conversion efficiency.[4] Silicon is perhaps the most studied solar absorber,[2] with high-efficiency photovoltaic modules already commercialized; however, costly processing and manufacturing hinders their large-scale deployment.[5,6] Consequently, there has been a push toward the development of high-efficiency solution-processed photovoltaics,[7] with dye-[8] and quantum dot-sensitized,[9-11] colloidal quantum dot,[12] organic,[13] copper-indium-gallium-selenide and copper-zinc-tin-sulfide,[14] and, most recently, organic/inorganic perovskite[15,16] solar cells already demonstrating impressive conversion efficiencies.

While inexpensive and efficient photovoltaic devices would mark a great advance toward reducing our reliance on fossil fuels, the intermittent nature of sunlight necessitates the storage of the photogenerated electricity. The performance of rechargeable lithium ion batteries has

advanced considerably over recent years, but further improvements in energy density and cycling stability together with lower overall cost are still needed to meet our ever-increasing power demands.[17,18] An attractive alternative solution would be to store the energy from sunlight in the chemical bonds of portable molecular fuels,[19] such as hydrogen gas[1,20-22] or simple hydrocarbons.[23-25] These molecular fuels could then be stored, transported, and ultimately consumed on demand using a light-weight fuel cell device to efficiently generate electricity with few harmful byproducts.[26,27] Hydrogen is perhaps the most attractive molecular fuel, as it can be produced through the environmentally-benign electrochemical splitting of water and consumed in the presence of oxygen (from air) to yield electrical power and water as its only products.[27] In particular, hydrogen fuel obtained by water electrolysis is free of the contaminants found in hydrogen gas from reformed hydrocarbons that can poison traditional fuel cell electrocatalysts, reducing their efficiency and lifetime.[26] Furthermore, by coupling a semiconducting light absorber with suitable electrocatalysts for hydrogen and oxygen evolution, it becomes possible to mimic photosynthesis by using solid, inorganic materials to convert sunlight into hydrogen fuel.[20,22,28-30]

Given the considerable attention that they have already received from the research community, both photovoltaic energy conversion and water electrolysis are fairly mature technologies, and one could imagine pairing the best solar cell devices with the best electrocatalysts to efficiently produce solar fuels; however, as is similarly the case for photovoltaics, issues of scalability and economic feasibility preclude such a simple solution.[31] Moreover, these technologies face constant competition from relatively inexpensive, well-established, and energy-dense fossil fuels.[1] To become economically competitive, solar fuel devices and liquid-junction photoelectrochemical solar cells must operate efficiently using low-

cost and earth-abundant materials. This requirement is not met by present energy conversion technologies, which often rely on noble metal or noble metal-containing electrocatalysts to drive their relevant redox reactions. For example, platinum has long been a favored electrocatalyst for several important electrochemical reactions due to its versatility, high activity, and chemical inertness,[32] but its low abundance in the Earth's crust cannot support large-scale application.[33] Therefore, contemporary renewable energy technologies that rely on noble metal and noble metal-containing electrocatalysts ideally should transition to low-cost, earth-abundant alternatives if they hope to become cost competitive with fossil fuel-based energy sources.[34]

In this review, we seek to first provide a high-level overview of electrocatalysis and its central role in various renewable energy technologies. Due to the broad scope of this topic, we will largely limit our discussion to inorganic heterogeneous electrocatalysts and the cathodic reactions where there are clear opportunities for earth-abundant electrocatalysts: the hydrogen reduction reaction (HER), the oxygen reduction reaction (ORR), and the redox reactions in regenerative liquid-junction photoelectrochemical solar cells (Fig. 1). Carbon dioxide and monoxide reduction are relatively nascent fields of heterogeneous electrocatalysis that could similarly benefit from the development of highly selective earth-abundant inorganic electrocatalysts, but they have been thoroughly reviewed elsewhere,[23-25] and because noble metal-containing electrocatalysts are generally not employed in these applications, they will not be discussed in detail here.

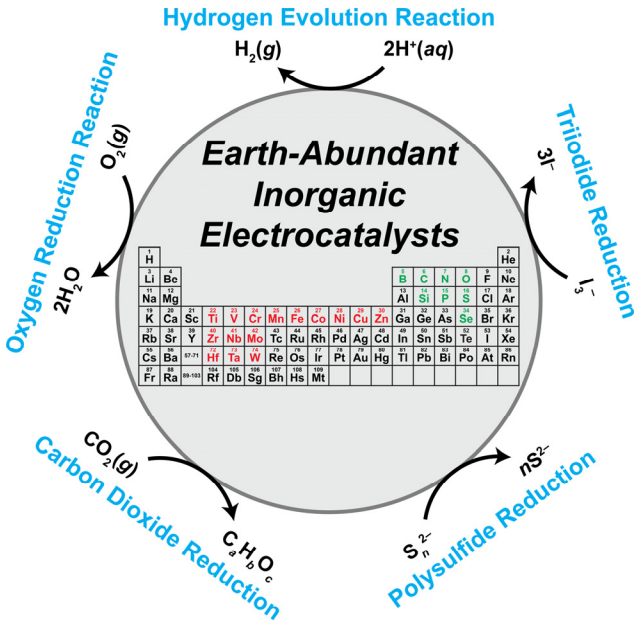

Fig. 1 Schematic illustration of selected energy conversion applications for earth-abundant inorganic electrocatalysts. The earth-abundant transition metal elements primarily considered in this review are indicated in red in the periodic table, while the non-metal elements in green define the specific families of electrocatalytic inorganic transition metal compounds that are discussed here.

We will then survey recent work toward developing new high-performance, earth-abundant inorganic electrocatalysts, focusing our discussion on promising classes of materials as defined by their chemical compositions. Although carbonaceous electrocatalysts, such as graphene and graphene derivatives,[35] carbon nanotubes (CNTs),[36,37] and conductive polymers,[38,39] have recently emerged as effective electrocatalysts, they lie outside the scope of this review. Homogeneous molecular catalysts have also witnessed significant development in recent years, but they have been thoroughly reviewed elsewhere[34,40-46] and will not be emphasized here. For each class of materials, we will try to highlight major advances and the prevailing trends in development. The key challenges facing earth-abundant electrocatalysts will

then be detailed, along with a discussion of current and emerging strategies for improving the performance of such catalysts. Lastly, we will offer our perspectives on the development of earth-abundant electrocatalysts in hopes of lighting a path toward achieving performance competitive with their noble metal-containing analogues. Because of the tremendous progress and accelerating rate of publication in this rapidly emerging research field, we cannot ensure that this review encompasses the full body of work related to this topic, particularly those works most recently published; instead, we seek to highlight the key themes and seminal advances that have influenced the primary directions of research.

2. Electrocatalysis and its central role in electrochemical energy conversion

Any process that involves a chemical transformation induced by the transfer of electrical charge to a substrate molecule can proceed efficiently only if the rates of charge transfer and chemical reaction are high. To maximize the efficiency of such transformations, catalysts are commonly employed to facilitate both charge transfer and subsequent chemical reaction, accelerating their respective rates. The specific forms of these catalysts, as well as their methods of integration and utilization, often vary, as discussed later, but their function is always to increase the rate of a chemical transformation reaction.

As a result, when developing electrochemical systems for efficient energy conversion based on solid/liquid or solid/gas interfaces, electrocatalysis is a key consideration.[32] Electrode materials are chosen primarily based on their ability to drive the redox reactions of interest with

low energy loss, which demands minimization of the electrochemical cell voltage, V, generally given by

$$V = \Delta E_{eq} - \eta_a + \eta_c - IR \quad (1)$$

where ΔE_{eq} is the difference between the equilibrium electrode potentials; η_a and η_c represent the total overpotentials (including the overpotential associated with mass transport) at the anode and cathode, respectively; and IR is the voltage drop across all current-carrying components of the electrochemical cells, as determined by Ohm's law. An effective electrocatalyst reduces the cell voltage by minimizing the electrode overpotential, η, defined as the deviation of the applied potential from the equilibrium potential, which is related to the current density, J, by the Tafel equation,

$$|\eta| = \frac{2.3RT}{\alpha nF} \log \frac{J}{J_0}. \quad (2)$$

In this relationship, η is minimized by a low Tafel slope ($b = 2.3RT/\alpha nF$, often expressed in mV decade^{-1}, where R is the ideal gas constant, T is the absolute temperature, α is the electrochemical transfer coefficient, n is the number of electrons involved in the electrode reaction, and F is the Faraday constant), which gives the applied overpotential necessary to change the current density by an order of magnitude, and a large exchange current density (J_0), which indicates the electrode kinetics toward the redox reaction of interest. Therefore, electrocatalysts with high intrinsic activity toward a specific redox process are characterized by a low Tafel slope and a high exchange current density.

Consequently, electrocatalysts and electrocatalytic electrode materials are primarily selected based on their ability to reduce overpotentials, regardless of the specific application. For example, in liquid-junction photoelectrochemical dye- and quantum dot-sensitized solar cell

(DSSC and QDSSC, respectively) devices, the counter electrode material and/or electrocatalyst must be carefully selected based on its intrinsic activity toward the redox couple in solution that facilitates hole transport and the regenerative flow of photocurrent. In the case of DSSCs, the counter electrode must maximize the rate of triiodide (I_3^-) reduction (Fig. 2a); for QDSSCs, polysulfide species (S_n^{2-}) in solution must be efficiently reduced at the counter electrode (Fig. 2b).

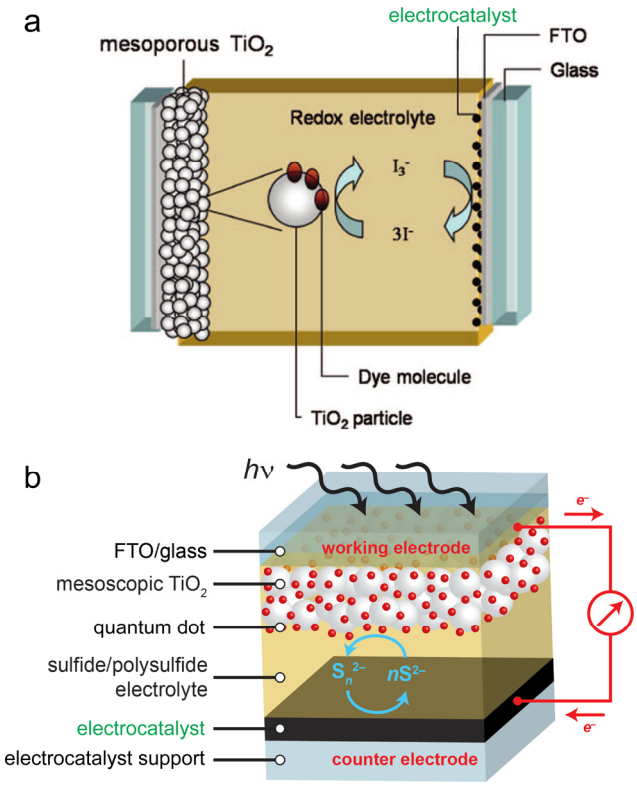

Fig. 2 Schematic illustrations of the respective roles of the electrocatalyst at the counter electrode of (a) dye- and (b) quantum dot-sensitized solar cells. Panels (a) and (b) adapted from Refs. 8 and 138, respectively, with permission from the American Chemical Society.

For the generation of hydrogen fuel through water electrolysis, summarized by the equation

$$2H^+(aq) + 2e^- \rightarrow H_2(g) \qquad (3)$$

the cathode must be sufficiently active toward the HER to reduce protons at low overpotentials. In the case of the HER, in-depth mechanistic studies have determined the relationship between the Tafel slope and the rate-limiting step of electrocatalysis,[47] assuming a constant coverage of adsorbed hydrogen over a range of potentials. Specifically, a Tafel slope of approximately 120 mV decade^{-1} indicates that the discharge step (Volmer reaction),

$$H^+(aq) + e^- + * \rightarrow H^*_{ad} \quad (4)$$

where a free proton in solution adsorbs to an active site at the electrocatalyst surface (denoted here by an asterisk) with the transfer of an electron, is rate limiting. A Tafel slope of about 40 mV decade^{-1} suggests that the electrochemical desorption step (Heyrovský reaction),

$$H^*_{ad} + H^+(aq) + e^- \rightarrow H_2(g) + * \quad (5)$$

where a free proton in solution is simultaneously reduced and reacted with an adsorbed hydrogen atom to form $H_2(g)$, is rate limiting. A Tafel slope of 30 mV decade^{-1} indicates that the Tafel recombination step (Tafel reaction),

$$2H^*_{ad} \rightarrow H_2(g) + 2* \quad (6)$$

where two adjacent adsorbed hydrogen atoms combine to give $H_2(g)$, is rate limiting. Hydrogen evolution electrocatalysis typically proceeds through either reactions (4) and (5) (Volmer–Heyrovský mechanism) or (4) and (6) (Volmer–Tafel mechanism), but both can occur simultaneously, leading to intermediate Tafel slopes. Note that the HER can proceed in acidic, neutral, or basic conditions, and that the specific requirements for electrocatalysts in these different environments—primarily in terms of their intrinsic activity and stability—can vary.

Similarly, in the proton exchange membrane fuel cells that convert hydrogen fuel to electricity, as well as in other types of fuel cells, the cathode must exhibit high activity toward the four-electron reduction of dioxygen to water,

$$O_2(g) + 4H^+(aq) + 4e^- \rightarrow 2H_2O \,. \qquad (7)$$

In particular, achieving dioxygen reduction at low overpotentials remains a great challenge, even when using noble metal electrocatalysts, due to the strength of the O=O double bond relative to that of the metal–oxygen bond.[27,48] Furthermore, ORR electrocatalysts with poor selectivity can yield hydrogen peroxide side products that are detrimental to fuel cell stability and lifetime.

When assessing the viability of a candidate electrocatalyst material, its performance is commonly compared to that of its competitors as well as to the state of the art. The Tafel slope and exchange current density of the electrocatalyst provide insights into its intrinsic activity. Furthermore, characteristics related to practical application, such as the onset potential for catalytic current or the overpotential required to achieve a certain catalytic current density (with 10 mA cm^{-2} being the most common standard used for HER electrocatalysis), are usually analyzed when evaluating electrocatalyst performance. The *IR* correction of current density–voltage data—which involves subtraction of the voltage drop due to the overall series or internal resistance, usually determined through electrochemical impedance spectroscopy or the current interrupt method[49]—prior to analysis enables a fair comparison of electrocatalyst performance. These aspects should be considered together with the electrocatalyst loading (typically expressed in mg cm^{-2}) and the effective electrochemical surface area (often determined either by probing the electrode double-layer capacitance[49-51] or through the physisorption of gas molecules) to ensure that electrocatalyst performance is accurately compared. Knowing the areal density of

active sites for catalysis also permits calculation of the turnover frequency (*i.e.*, the number of chemical transformations that can be driven by a catalytic site per unit time), a measure of intrinsic activity most commonly used to evaluate molecular catalysts. Standardization of these procedures into a common protocol for electrocatalyst benchmarking (as has recently been done for oxygen evolution electrocatalysts[52]) permits their objective comparison. Long-term stability of the electrocatalysts under both operating and shutdown conditions, which permits stable operation over extended periods of time, is also critically important. Such stability considerations encompass both the chemical and electrochemical stability of the electrocatalyst material as well as the mechanical stability of the entire electrode structure itself. Additional factors, such as cost and ease of synthesis, together with overall stability, also inform the selection of electrocatalysts and/or electrode materials, but in all cases, electrocatalytic activity takes precedent.

The need for electrocatalysts to be electrically contacted can also place restrictions on their preparation, and, in a sense, this may have naturally led to the early identification of bulk noble metals as superior electrocatalysts. Although homogeneous catalysts can be freely diffusing in solution, heterogeneous electrocatalysts must be interfaced with a solid support that is sufficiently conductive to allow the passage of electrical current to the electrocatalysts. Common electrocatalyst supports include graphite, glassy carbon, metal foils, and transparent conducting oxide films on glass, but other conductive materials are suitable so long as they are inert in their respective electrochemical environments. Alternatively, sufficiently robust and metallically conducting electrocatalysts (including certain transition metals, alloys, and compounds) can double as the electrode material itself, eliminating the need for a conductive support. For this reason, the transition metals were among the first materials explored for electrode applications. Researchers quickly identified the noble metals, particularly platinum, as

optimal electrode materials, due to their high electrocatalytic activity, chemical inertness, versatility, high conductivity, and resistance to oxidation.[32] Consequently, noble metal electrodes have long served as a trusted and reliable platform for electrochemical studies, with other transition metals failing to achieve comparable levels of performance and stability. For example, in the case of triiodide reduction for regenerative liquid-junction DSSCs, platinum continues to serve as the benchmark counter electrode material, though other materials have recently been explored.[8,53-55] Similarly, the transition metals exhibit a Sabatier trend in HER electrocatalytic activity (yielding a so-called "volcano" plot), in accordance with theoretical predictions,[56] with platinum and other platinum group metals exhibiting the highest activity (Fig. 3a).[57] Likewise, in agreement with experimental observation, calculations predict platinum to have the highest ORR activity among the transition metals (Fig. 3b).[58] In each of these cases, the high electrocatalytic activity of platinum results from energetically favorable interactions with the relevant redox species in solution. Systematic surveys of electrocatalytic activity such as those shown in Fig. 3 help to reveal design principles that can guide the development of alternative electrocatalysts with the potential to compete with platinum.

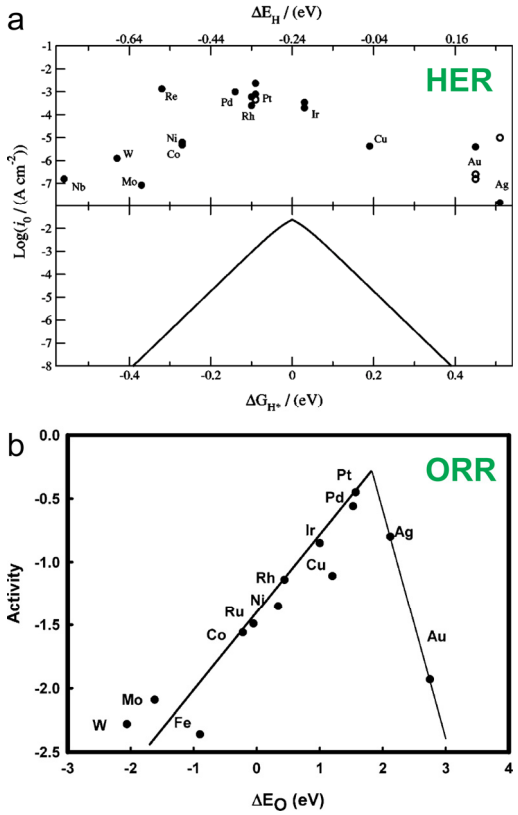

Fig. 3 Trends in the electrocatalytic activity of various transition metals toward the hydrogen evolution reaction (HER) and oxygen reduction reaction (ORR). (a) Experimental (top) and theoretical (bottom) semi-log plots of the exchange current density for the HER at different transition metal surfaces plotted as a function of the calculated hydrogen chemisorption energy per atom (ΔE_H; top axis) and the free energy for hydrogen adsorption ($\Delta G_{H*} = \Delta E_H + 0.24$ eV; bottom axis). Reproduced from Ref. 57 with permission from The Electrochemical Society, Inc. (b) Theoretical activity of various close-packed transition metal surfaces toward the ORR plotted as a function of the oxygen binding energy (ΔE_O). Reproduced from Ref. 58 with permission from the American Chemical Society.

3. Earth-abundant inorganic electrocatalysts

Many earth-abundant inorganic transition metal compounds have found use as heterogeneous catalysts in industrial hydrotreating and reforming processes.[59,60] For example, ruthenium-based catalysts for the hydrodesulfurization (HDS) and hydrodenitrogenation (HDN) of petroleum have been successfully replaced by sulfide catalysts containing molybdenum, cobalt, nickel, and/or tungsten.[61] Also, supported earth-abundant transition metal oxide catalysts have been implemented in a number of industrial processes and often serve as model systems to study catalytic transformations.[62] The extensive study and development of these and other industrially-relevant earth-abundant catalysts made them obvious candidate electrocatalysts for emerging energy conversion applications. Consequently, a number of the earth-abundant electrocatalysts discussed in this section have an interesting lineage that in some way traces back to alternative hydrotreating and reforming catalysts. Owing to the burgeoning interest in inexpensive electrochemical energy conversion, however, the variety of earth-abundant inorganic electrocatalysts currently under consideration has grown beyond these historical confines.

From a sustainability and scalability perspective, the need for electrocatalysts composed of elements in high terrestrial abundance is evident, but there are several other considerations that inform the selection of specific electrocatalyst materials and their methods of preparation. In addition to being low-cost and earth-abundant, we would prefer that electrocatalyst materials be environmentally benign. By using materials of low environmental impact, such as those composed primarily of rock-forming elements, disposal concerns are assuaged. Furthermore, it would not be necessary to salvage or recycle the materials in devices containing earth-abundant electrocatalysts at the end of their lifetime, as is commonly done for devices containing noble metals. For economic and throughput reasons, the preparation of such materials should also be

based on highly scalable procedures. For example, low-yield syntheses should be replaced with large-scale preparations, where possible, to ensure that electrocatalyst materials can be produced in quantities necessary to meet commercial demand. Similarly, highly specialized processing steps should be eliminated or at least minimized to avoid production bottlenecks. Lastly, the electrocatalyst support should be selected based on its capacity for both maximizing performance and minimizing cost. For example, efficient earth-abundant electrocatalysts demonstrated on metal foil, transparent conducting oxide/glass, or glassy carbon supports might instead be prepared on cheap yet highly conducting graphite substrates to reduce cost. To further boost electrocatalyst performance, high surface area supports such as carbon fiber paper could also be used.

The wide array of earth-abundant inorganic electrocatalysts that have been investigated so far can be most logically categorized based on their elemental composition. We will begin our survey by briefly discussing the molecular systems that have largely inspired the use of transition metals and their compounds as electrocatalysts. We will then outline the use of transition metals and their alloys for electrocatalytic applications, before moving on to the various classes of transition metal compounds. Note that, within this section, the phrase "transition metal" implies "non-noble transition metal" (referring to those elements indicated in red in Fig. 1), unless explicitly indicated otherwise. In each subsection, central themes and trends in materials development will be described, as will key demonstrations of electrocatalysis for energy conversion.

3.1. Homogeneous and supported molecular systems.

Inspired by natural enzymes capable of efficiently catalyzing complex redox reactions, such as the photosynthetic reduction of carbon dioxide and oxidation of water to respectively produce carbohydrates and molecular oxygen,[63] great efforts have been made to design, synthesize, and characterize molecules that can split water (or other hydrogen-containing substrates) to generate hydrogen fuel.[40] Most recently, efforts have been primarily directed toward developing molecular catalysts that exclusively contain earth-abundant transition metals (*e.g.*, Fe, Co, Ni, and Mo), with particular attention toward those that can be coupled to light-absorbing semiconductors to drive the photoelectrochemical production of hydrogen fuel.[34,42-44,46] Similarly, molecular catalysts for the electrochemical reduction of carbon dioxide have been investigated.[23,45] Molecular catalysts can operate as free complexes in solution or can be covalently grafted to a conductive support.[34,42,46,64] Biomimetic incomplete cubane-type $[Mo_3S_4]^{4+}$ molecular electrocatalysts supported on highly ordered pyrolytic graphite or carbon black have been shown to exhibit high HER electrocatalytic activity.[65] When drop-cast on light-absorbing *p*-type silicon photocathodes, these cubane-like molecular clusters enable solar hydrogen evolution.[66] Despite their high intrinsic activity, such molecular catalysts often suffer from low overall performance and relatively poor stability. The possibility of unraveling the mechanisms of complex catalytic processes, however, motivates study of these molecular catalysts.[43] These insights could then lead to design principles that help guide the development of inorganic heterogeneous electrocatalysts with superior performance and long-term stability.[41] Indeed, the careful study of molecular systems has informed the development of several earth-abundant heterogeneous electrocatalysts that will be henceforth discussed. Due to the vast body of work on molecular catalysts for alternative energy applications, we cannot provide an

exhaustive overview here; instead, we refer the reader to the many review articles that summarize recent progress in this field.[34,40-46]

3.2. Transition metals and their alloys.

The superior intrinsic activity and stability of noble metal electrodes has mostly excluded the use of elemental earth-abundant transition metal electrodes for energy conversion applications. The early realization that most transition metals are reactive and/or susceptible to corrosion in many electrolytes, both aqueous and non-aqueous, has led to a strong preference for inert noble metal electrodes, even in cases where their high intrinsic activity is not needed. For example, several transition metals have been investigated as alternative counter electrode materials in DSSCs in hope of replacing platinum, including nickel, molybdenum, and tungsten, but all suffered from inferior activity and corrosion caused by the iodide species in the electrolyte.[53] Similarly, several transition metal counter electrodes have been employed in QDSSCs that employ the sulfide/polysulfide redox couple in aqueous solution. In contrast to their behavior in DSSCs, it was found that reactivity between certain transition metals and dissolved sulfur species leads to the rapid formation of a transition metal sulfide coating, which, remarkably, catalyzes polysulfide reduction more effectively than even platinum (see additional discussion in Section 3.4).[67]

The measurement of the HER electrocatalytic activity of the transition metals in both acidic[68] and alkaline[69] conditions has helped to guide the development of state-of-the-art earth-abundant inorganic electrocatalysts. These activities, as determined from the exchange current density or the overpotential at a standard current density, were found to correlate with the work function of the transition metal in both acid and base, with the high work function noble metals

consistently exhibiting the highest activities.[68,69] Other possible correlations between the rate of HER and the physical properties of elemental electrodes have also been investigated.[70] These results suggest that the electronic properties of a material factor heavily into its anticipated electrocatalytic activity, and that certain physical properties could predict trends in catalytic activity. Establishing such trends for redox reactions central to other energy conversion applications could similarly guide the development of improved electrocatalysts.

Noting the low activity of transition metal electrocatalysts as compared to the noble metals in most energy conversion applications, researchers began investigating the activity of transition metal alloys. In the case of hydrogen generation through electrocatalytic water splitting, "volcano" plots of transition metal activity (Fig. 3a) suggested that there could be synergistic benefits of using alloy or multimetallic electrodes that could, through the cooperative interactions of metal species with differing hydrogen affinity, emulate or even improve upon the highly active surfaces of noble metal electrodes.[71-74] Specifically, alloying of transition metals is expected to tune the *d*-band electron filling, Fermi level energy, and interatomic spacing, all of which could impact the affinity of the alloy electrocatalyst toward the adsorbate species of interest.[32,75] One of the earliest observations of this effect was for the Ni–Mo alloys, which exhibit superb activity toward the HER in alkaline conditions.[34,76] Ni–Mo alloy coatings prepared on nickel mesh substrates have been shown to achieve a current density of 1 A cm^{-2} at a low cathodic overpotential of only 83 mV vs. the reversible hydrogen electrode (RHE).[76] Other transition metal alloys, including Ni–V, Ni–Fe, Ni–W, Co–Mo, and Fe–Mo, similarly exhibited high activity toward the HER in alkaline conditions, although not as high as that of Ni–Mo.[77,78] Remarkably, these electrocatalytic alloy films retain their high performance for at least one year of continuous operation in alkaline conditions, with no decay in activity under shutdown

conditions.[77] More recently, a synthesis for unsupported Ni–Mo nanopowders was developed, and Ni–Mo nanopowder films cast on titanium foil electrodes exhibited exceptional activity toward the HER in alkaline conditions at a substantially reduced electrocatalyst mass loading.[79] Moreover, the electrodeposition of Ni–Mo electrocatalyst particles on silicon photoelectrodes has been demonstrated, enabling an integrated photoelectrochemical system capable of storing solar energy in the form of hydrogen fuel.[80,81]

Following the observation of high HER electrocatalytic performance from Ni–Mo catalyst films, the activity of several ternary transition metal alloys was similarly investigated. Consistent with the relatively high HER activity of Ni and the Ni–Mo alloys, the highest performing ternary alloy electrocatalysts typically contain both Ni and Mo. Ternary Ni–Mo–Cd electrocatalyst films prepared on iron substrates by electrodeposition were claimed to possess very high intrinsic activity toward the HER in alkaline conditions, with Tafel slopes as low as 26–30 mV decade^{-1}.[82] Despite incorporation at only 1 at.%, the presence of cadmium in the ternary alloy was thought to facilitate hydrogen evolution by a desorptive mechanism due to adsorbed hydrogen or surface hydride species.[82] Various other ternary Ni–Mo-derived alloys have also been explored as HER electrocatalysts in alkaline conditions, including alloys containing Fe, Cu, Zn, W, Co, or Cr, with the Ni–Mo–Fe alloy exhibiting the highest performance among these.[83] To illustrate the real-world applicability of these ternary transition metal alloy HER electrocatalysts, Ni–Mo–Zn was recently integrated into a monolithic photoelectrochemical water-splitting "artificial leaf" device.[29,84]

3.3. Transition metal oxides.

Despite their prevalence as industrial catalysts,[62] the binary transition metal oxides generally do not find use as electrocatalysts due to their poor electrical conductivity and low chemical stability (particularly in acidic conditions) among transition metal compounds.[39] However, there are several successful demonstrations of transition metal oxide electrocatalysts for energy conversion.[39,85] Many transition metal oxides have decent ORR activity in alkaline media.[39] For example, manganese oxide (MnO_2) nanostructures have been shown to be effective ORR electrocatalysts in basic conditions,[86] and spinel-phase (AB_2O_4) Co–Mn–O nanoparticles have been demonstrated as bifunctional electrocatalysts for both the oxygen reduction and evolution reactions.[87] Similarly, spinel-phase lithium cobalt oxide ($LiCoO_2$) is an efficient oxygen evolution electrocatalyst, and chemically delithiated $Li_{1-x}CoO_2$ exhibits both oxygen reduction and evolution activity.[88] Interestingly, the delithiation procedure allows the $Li_{1-x}CoO_2$ electrocatalyst to be tuned for optimal bifunctional activity (which occurs for $x = 0.5$).[88] Perovskite-phase (ABO_3) oxides have also been investigated as ORR electrocatalysts, with established design principles and trends serving as predictors of electrocatalytic activity.[89] By preparing transition metal oxide electrocatalysts on a compatible conductive support, their performance and stability can often be dramatically improved.[90] For example, cobalt oxide (Co_3O_4) nanoparticles exhibit little ORR activity on their own; however, this activity is greatly enhanced when they are grown on a reduced graphene oxide (RGO) support.[91] In this case, favorable chemical and electronic coupling between RGO and the Co_3O_4 nanoparticles leads to a synergistic enhancement of electrocatalytic activity (see additional discussion in Section 5.4).[91] Similarly, solution-grown magnetite (Fe_3O_4) and core/shell nickel/nickel oxide (Ni/NiO) nanoparticles anchored on metallically conducting cobalt diselenide ($CoSe_2$) nanobelts have been shown to exhibit enhanced activity toward the ORR[92] and HER,[93] respectively. Niobium oxides

have also been demonstrated as stable, efficient ORR electrocatalysts in acidic conditions.[94] More recently, several niobium oxides have emerged as effective counter electrode materials in DSSCs, with tetragonal NbO_2 counter electrodes enabling power conversion efficiencies higher than that of equivalent devices assembled with a platinum counter electrode.[95] Similarly, faceted iron oxide (α-Fe_2O_3, hematite) nanoparticles were theoretically predicted to exhibit high activity toward triiodide reduction, and films thereof were subsequently demonstrated to compete with platinum counter electrodes in DSSC devices.[54]

3.4. Transition metal chalcogenides.

The transition metal chalcogenides[96,97] make up the largest class of earth-abundant electrocatalysts. Initial studies on the electrocatalytic properties of metal chalcogenide electrodes mostly grew out of the investigation of single-crystalline semiconducting metal chalcogenide photoelectrodes, such as CdS, CdSe, CdTe, ZnSe, and Bi_2S_3.[98-101] More recently, these semiconducting materials have been synthesized as nanocrystalline quantum dots and used as light-absorbing inorganic sensitizers for the wide band gap semiconductor films in QDSSCs.[9-11] In these studies, it was found that the sulfide/polysulfide redox electrolyte prevented metal chalcogenide photoelectrode corrosion, thereby making it the preferred hole mediator.[99-101] Earlier works had identified platinum and gold as the most chemically stable electrode materials in the sulfide/polysulfide electrolyte, with high surface area platinum electrodes showing the best performance,[102] but it was later found that sulfur species poison platinum electrodes by irreversibly adsorbing to their surface, substantially reducing their electrocatalytic activity.[103] It was known that sulfur species in the sulfide/polysulfide electrolyte rapidly attack non-noble transition metals such as nickel and tungsten, forming a metal sulfide surface coating,[102] but decades would pass before such high surface area metal sulfide films were discovered to possess

substantially higher intrinsic activity toward the sulfide/polysulfide redox couple than platinum.[67] Cuprous sulfide (Cu_2S) spontaneously formed on copper or brass foils was identified as the most active transition metal sulfide electrocatalyst toward the sulfide/polysulfide redox couple; however, its chemical and mechanical instability in the sulfide/polysulfide electrolyte could lead to poisoning of the photoactive electrode and, eventually, complete disintegration.[67] The mechanical stability of Cu_2S-based electrodes was improved through the preparation of a Cu_2S–RGO composite,[104] which has been used as the electrocatalytic counter electrode material in liquid-junction QDSSCs to give solar light-to-electricity power conversion efficiencies as high as 6.6%.[105]

For QDSSCs, the chemical incompatibility of platinum electrodes with the sulfide/polysulfide electrolyte naturally led to the exploration of alternative, earth-abundant transition metal chalcogenide electrocatalysts for polysulfide reduction. However, in the case of DSSCs that employ the iodide/triiodide redox couple, platinum counter electrodes consistently enable the highest device performance. Here, the challenge is to identify earth-abundant electrocatalysts for triiodide reduction that can not only withstand the corrosive iodide/triiodide electrolyte, but also compete with the exceptional activity of platinum. Several transition metal chalcogenides meet these requirements. Furthermore, many transition metal chalcogenides have been investigated as replacements for noble metal electrocatalysts for the HER and ORR. Within this section, the transition metal chalcogenides will be discussed in subgroups defined by their structure types, with most being either layered or cubic pyrite-phase materials. The emerging amorphous transition metal chalcogenide electrocatalysts—which are characterized by their *lack* of a well-defined structure—will also be briefly discussed, as will materials that do not fall into one of these three main subgroups.

3.4.1. Layered materials. The layered transition metal dichalcogenide (TMD) materials,[106] with a general chemical formula of MX_2 (M being a transition metal, and X typically being S or Se), make up perhaps the most widely studied family of earth-abundant inorganic electrocatalysts.[107,108] Among the many layered TMD electrocatalysts that have recently been used for energy conversion, molybdenum disulfide (MoS_2) was one of the first to emerge, and it continues to serve as a prototypical example.[109] In 2005, a pioneering work investigating the energetics of hydrogen evolution from a [NiFe]-hydrogenase system and the FeMo cofactor active site of nitrogenase suggested MoS_2 as a possible inorganic analogue of these natural systems.[110] The electrocatalytic activity of MoS_2 nanoparticles dispersed on carbon supported the computational model, with the edge sites of the MoS_2 layers identified as being most catalytically active toward the HER (as is also the case in HDS).[110] Scanning tunneling microscopy studies performed on MoS_2 nanoparticles on a Au(111) support have served to unequivocally establish the edge sites of MoS_2 as being most active for HER (Fig. 4a), exhibiting turnover frequencies comparable to those of high-activity noble metals.[111] The activity of these MoS_2 edge sites can also be enhanced through the introduction of cobalt "promoter" species.[112] In an effort to resolve the exact nature of the active edge sites of MoS_2, a well-defined Mo^{IV}-disulfide molecular mimic has been prepared and characterized both structurally and electrochemically (Fig. 4b).[113]

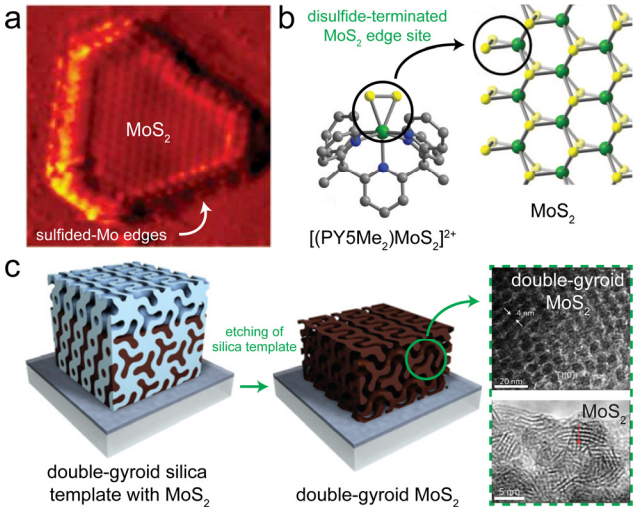

Fig. 4 Identification of the edge-site activity of MoS_2 toward the HER, and an example of the engineering strategies used to maximize the exposure of these edge sites. (a) Atomically-resolved scanning tunneling microscopy image of a MoS_2 nanoparticle, showing the sulfided Mo-edge sites that exhibit superior HER electrocatalytic activity (60 Å by 60 Å, 1.0 nA, 300 mV). (b) Molecular analogue (left) of the triangular disulfide-terminated MoS_2 edge sites (right). (c) Abbreviated scheme for the synthesis of double-gyroid mesoporous MoS_2 engineered to preferentially expose edge sites for enhanced HER activity. Panels a and b adapted from Refs. 111 and 113, respectively, with permission from the American Association for the Advancement of Science. Panel c adapted from Ref. 125 with permission from Macmillan Publishers.

Although the layered TMDs tend to preferentially form closed fullerene-like or nanotubular structures to minimize the presence of dangling bonds at their edges,[114] various synthetic[51,115-124] and engineering[125,126] strategies have been applied to proliferate the exposed edge sites of the layered TMDs for increased electrocatalytic activity. The introduction of defects within the layered TMD crystal structure can also generate new active edge sites for catalysis, enhancing its performance.[120,121] Alternatively, the morphology of the layered TMD material can

be controlled during synthesis to maximize the exposure of edge sites. For example, by engineering the synthesis of MoS_2 to yield a high surface area, mesoporous, double-gyroid morphology, the fraction of exposed MoS_2 edge sites has been increased, boosting its HER electrocatalytic performance (Fig. 4c).[125]

Furthermore, it has recently been shown that chemical exfoliation of layered TMDs can dramatically increase the availability of active edge sites while simultaneously converting the as-synthesized MX_2 material from its thermodynamically-favored semiconducting 2H polymorph to its metallic 1T polymorph, granting enhanced electrocatalytic activity and electrical conductivity (Fig. 5a).[51,116,117] This strategy has been employed for nanostructures of both MoS_2[116] (Fig. 5b–c) and WS_2[51] (Fig. 5d–e) synthesized through chemical vapor deposition (CVD). The resulting 1T-MoS_2 and 1T-WS_2 nanosheets exhibit dramatically enhanced HER electrocatalytic performance as compared to their corresponding 2H polymorphs (Figs. 5f and 5g, respectively) despite the relatively low mass loading of these electrocatalyst materials. Specifically, reduced Tafel slopes are observed (43 mV decade^{-1} for the 1T-MoS_2 nanosheets, as indicated in the inset of Fig. 5f), and low cathodic overpotentials are required to achieve an electrocatalytic current density of 10 mA cm^{-2} (187 mV and 142 mV vs. RHE for 1T-MoS_2 and 1T-WS_2, respectively). Structural characterization and electrochemical studies confirm that the metallic 1T-MoS_2 and 1T-WS_2 nanosheets exhibit facile electrode kinetics, low-loss electrical transport, and an increased density of active sites for catalysis. These distinct and previously unexploited features of 1T-MX_2 make these metallic nanosheets highly competitive earth-abundant HER electrocatalysts. Note that, in these cases, the chemical nature of the MX_2 material plays a critical role in determining its electrocatalytic activity, *i.e.*, the metallic 1T-MX_2 nanosheets are intrinsically more electrocatalytically active than the semiconducting 2H-MX_2 nanostructures. Furthermore,

electrocatalytic 1T-MoS_2 has recently been coupled to a *p*-type silicon photoelectrode (Fig. 5h) to enable hydrogen evolution driven by solar energy (Fig. 5i).[127] Due to the exceptional HER activity of 1T-MoS_2 and the high-quality electrocatalyst–semiconductor interface enabled by the direct CVD growth of MoS_2 on silicon (followed by chemical exfoliation), a much higher photocurrent density for hydrogen evolution was achieved as compared to 2H-MoS_2 on silicon (Fig. 5i).

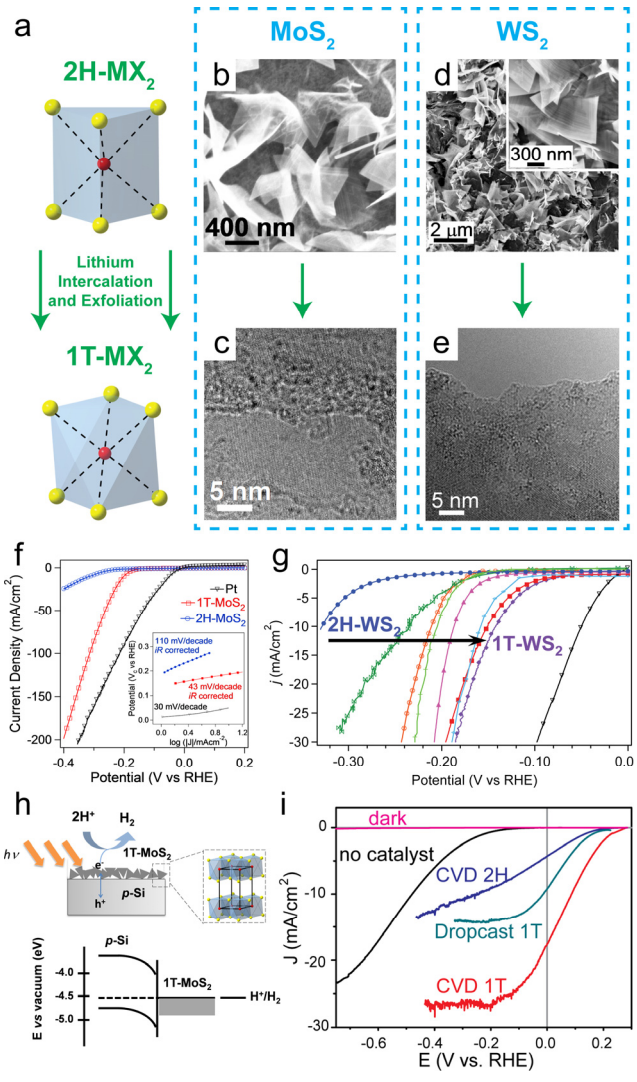

Fig. 5 Enhancement of the electrocatalytic activity of layered TMD nanosheets toward the HER through chemical exfoliation. (a) Intercalation of lithium into semiconducting 2H-MX_2 causes a

phase transition to the metallic 1T-MX_2 polymorph. This phase conversion has been demonstrated for the (b) 2H- to (c) 1T-MoS_2 and (d) 2H- to (e) 1T-WS_2 transitions, with subsequent exfoliation resulting in the formation of nanosheets. The combination of phase conversion and the exposure of additional catalytic edge sites results in a dramatic enhancement in HER electrocatalytic activity, as shown in the polarization curves for both (f) MoS_2 and (g) WS_2. The reduced Tafel slope of 1T-MoS_2 (panel f, inset) confirms that the improved performance is due to an increase in intrinsic activity along with a proliferation of edge sites for catalysis. (h) Direct growth of 1T-MoS_2 nanosheets on a *p*-type Si photocathode enables (i) efficient hydrogen evolution driven by solar energy. Panels a–c and f adapted from Ref. 116 and panels h–i adapted from Ref. 127, both with permission from the American Chemical Society; panels d, e, and g adapted from Ref. 51 with permission from The Royal Society of Chemistry.

Similarly, vertically aligned layers of MoS_2 can be grown on glassy carbon electrodes[118] and the spacing between layers can be tuned via the electrochemical intercalation of lithium ions (along with a concomitant 2H to 1T phase transition)[119] to grant enhanced activity toward the HER. Various chemical and engineering strategies can be used to improve the electrocatalytic activity of other layered TMDs, including WS_2,[128,129] $MoSe_2$,[118,130] and WSe_2.[130] The success of layered TMD electrocatalysts has further driven research efforts toward their preparation in nanostructured morphologies in order to leverage new or improved physical and chemical properties for energy conversion (and other) applications.[131-134] Additionally, the recent success of $NbSe_2$ nanosheets[135] and $MoSe_2$ particles[136] as triiodide reduction electrocatalysts in DSSCs and petaled MoS_2 as a polysulfide reduction electrocatalyst in QDSSCs[137] suggests that the layered TMDs likely exhibit high activity toward a broad range of redox processes.

3.4.2. Pyrite-phase materials. Recently, the cubic pyrite-phase TMDs[97] (MQ_2, where M is typically Fe, Co, or Ni and Q is commonly S or Se) have emerged as a new subclass of efficient electrocatalysts. As a rich family of mineral-forming compounds, the pyrites are expected to have high chemical stability, making them attractive for electrocatalytic applications. Perhaps inspired by industrial catalysts,[59] pyrite-phase materials have been exploited in sensitized solar cells and investigated as oxygen reduction and hydrogen evolution electrocatalysts. For example, metallic cobalt pyrite (CoS_2) polycrystalline thin films synthesized on insulating glass substrates (Fig. 6a) were shown to outperform platinum counter electrodes in QDSSCs filled with sulfide/polysulfide electrolyte, improving device performance and stability (Fig. 6b).[138] Electrochemical characterization further confirmed that CoS_2 exhibits both enhanced stability and activity toward polysulfide reduction as compared to platinum (Fig. 6c). Furthermore, pyrite-phase thin films of FeS_2, NiS_2, and a $(Ni,Fe)S_2$ alloy were also found to efficiently catalyze polysulfide reduction, with the intrinsic activity of NiS_2 exceeding that of CoS_2.[139]

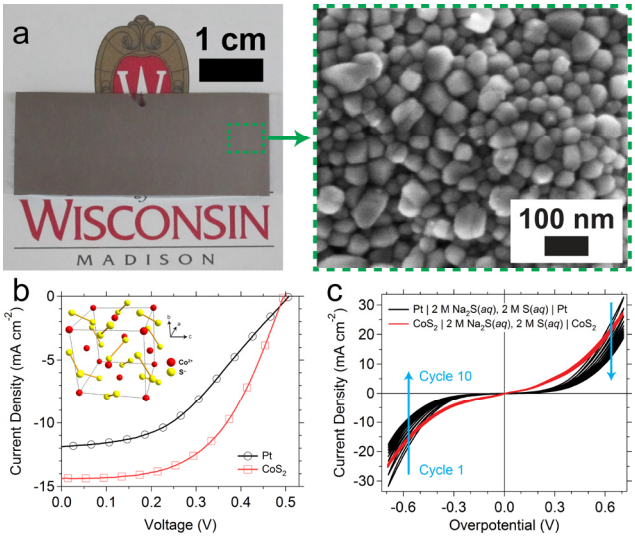

Fig. 6 Structural and electrochemical characterization of a metallic cobalt pyrite (CoS_2) thin film synthesized on glass and used as the counter electrode in a QDSSC. (a) Digital photograph showing the opaque CoS_2 film on the glass substrate (left), and scanning electron microscopy (SEM) image depicting the small-grain polycrystalline texture of the CoS_2 film (right). (b) Current density−voltage characterization of QDSSC devices filled with an aqueous sulfide/polysulfide (2 M S^{2-}/2 M S) electrolyte solution showing the enhanced performance of devices assembled with a CoS_2 counter electrode (red trace with square markers) rather than a Pt counter electrode (black trace with circle markers). The cubic pyrite crystal structure of CoS_2 is shown in the inset. (c) Cyclic voltammetric characterization of symmetrical electrochemical cells employing either CoS_2 (red trace) or Pt (black trace) electrodes and filled with sulfide/polysulfide electrolyte. Adapted from Ref. 138 with permission from the American Chemical Society.

Metallic CoS_2 also exhibits good stability and activity toward the iodide/triiodide redox couple, particularly when prepared in a high surface area morphology[50] or as a composite with graphene.[140] Remarkably, nanorod arrays[141] and nanocrystalline thin films[142] of iron pyrite (FeS_2), the semiconducting isostructural analogue of CoS_2,[143,144] on fluorine-doped tin oxide (FTO)/glass substrates have also been shown to compete with platinum counter electrodes in DSSCs. Similarly, high surface area CoS_2 hollow spheres drop cast on FTO/glass possess high electrocatalytic activity toward the disulfide/thiolate (T_2/T^-) redox couple sometimes used in DSSCs and QDSSCs, enabling DSSC performance exceeding that achieved with a platinum counter electrode.[145] Some pyrite phase transition metal diselenides, including $CoSe_2$ and $NiSe_2$, also show high electrocatalytic activity toward triiodide reduction.[136]

The ORR activity of the pyrite-phase (and other) transition metal chalcogenides was investigated as early as the 1970s,[146] but due to their comparatively low performance and durability, their activity went mostly unappreciated. It was not until much later that pyrite-phase transition metal disulfides including FeS_2, $(Fe,Co)S_2$, and CoS_2 were again investigated as model ORR electrocatalysts.[147,148] The family of pyrite-phase ORR electrocatalysts has since been expanded to include transition metal diselenides, with carbon-supported $CoSe_2$ nanoparticles exhibiting decent ORR activity in acidic conditions.[149] These works inspired further study of the pyrites for ORR, and it was recently found that nanocrystalline CoS_2 exhibits high activity and long-term stability under ORR operating conditions,[150,151] making it a promising candidate for the replacement of platinum in fuel cell systems.

As discussed previously, the active sites of natural hydrogenase and nitrogenase enzymes inspired work that led to the identification of the disulfide-terminated edges of MoS_2 (Fig. 4b) as active sites for HER electrocatalysis.[111] This activity was later confirmed through the study of molecular mimics.[113,152] These bio-inspired works suggest a particular beneficial role for disulfide (S_2^{2-}) anions in HER electrocatalysis, and the abundance of these species in all pyrite structures might contribute to the excellent electrocatalytic activity of the pyrites.[139] The noble metal-containing compound ruthenium disulfide (RuS_2) was one of the first pyrites identified as an active HER electrocatalyst in acidic conditions.[153] Because the pyrite structure accommodates compositional variation as a solid solution, allowing the formation of pyrite-phase alloys,[59] the effects of cobalt or nickel substitution in the RuS_2 lattice on electrocatalytic activity were investigated and optimized.[153] Interestingly, the binary pyrite-phase compounds CoS_2 and nickel pyrite (NiS_2) were also suggested as HER electrocatalysts,[153] but it was not until very recently that their specific HER activity was investigated. The high activity of CoS_2 toward the HER in

acidic conditions, confirmed using thin film electrodes (Fig. 7a), has been further enhanced by preparing CoS_2 microwire (Fig. 7b) and nanowire (Fig. 7c) arrays directly on a graphite support.[50] These comparisons showed that the introduction of micro- or nanostructuring to the CoS_2 material dramatically increased its performance (Fig. 7d) and stability (Fig. 7e) during hydrogen evolution by synergistically increasing the effective electrode surface area (leading to proliferation of active sites for electrocatalysis) and facilitating the release of evolved gas bubbles from the electrode surface (Fig. 7f), particularly for the microwire structures, as further discussed in Section 5.1.[50]

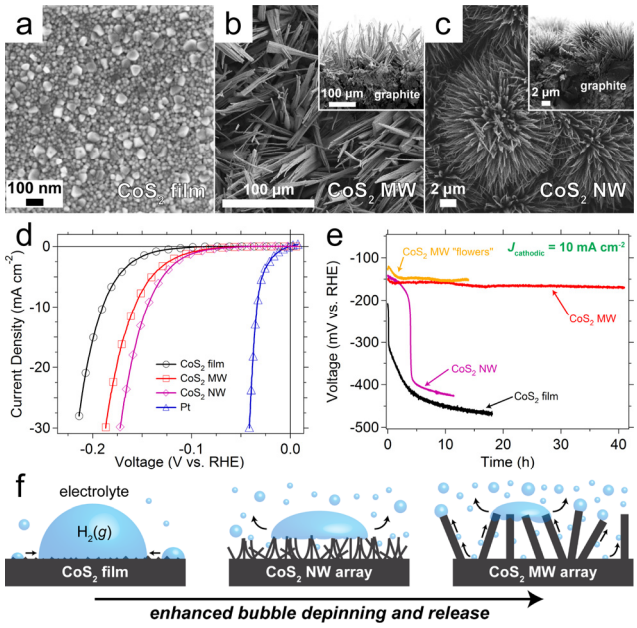

Fig. 7 Scanning electron microscopy images of cobalt pyrite (CoS_2) (a) film, (b) microwire (MW), and (c) nanowire (NW) electrodes. (d) Polarization curves showing the relative activity of as-prepared CoS_2 materials with different morphologies on graphite electrodes (film, open circles; MW, open squares; NW, open diamonds) toward the hydrogen evolution reaction in 0.5 M $H_2SO_4(aq)$, along with that of a Pt wire standard (open triangles). (e) Long-term stability measurements for representative CoS_2 film, NW, MW, and hierarchical MW "flower" electrodes

demonstrating the increased stability achieved through nanostructuring or, in particular, microstructuring. (f) Schematic depictions of CoS_2 NWs and MWs bursting the larger hydrogen gas bubbles that commonly pin at the surface of CoS_2 film electrodes, with the MWs most effectively wicking the evolved bubbles and maintaining the solid–liquid interface. Adapted from Ref. 50 with permission from the American Chemical Society.

The same micro- and nanostructuring strategy was also shown to enhance the performance of CoS_2-based electrodes toward triiodide and polysulfide reduction, suggesting their improved performance in liquid-junction DSSCs and QDSSCs, respectively.[50] Similarly, $CoSe_2$ films have been prepared on high surface area carbon fiber paper substrates to further increase their HER electrocatalytic performance.[154] Furthermore, the HER activities of various binary earth-abundant transition metal pyrites (and alloys thereof), including disulfides (Fig. 8a) and diselenides (Fig. 8b), were screened and compared to bring out trends in their performance. Based on a comparison of their Tafel slopes (Fig. 8c), it was found that thin films of CoS_2, $CoSe_2$, and NiS_2 on glassy carbon exhibited the highest intrinsic activities among the pyrites.[139,155] These recent works serve to substantially broaden the family of pyrite-phase HER electrocatalysts and establish that their activity can be modified through alloying, suggesting a potential pathway toward improving their intrinsic activity toward the HER and perhaps other electrochemical energy conversion processes.

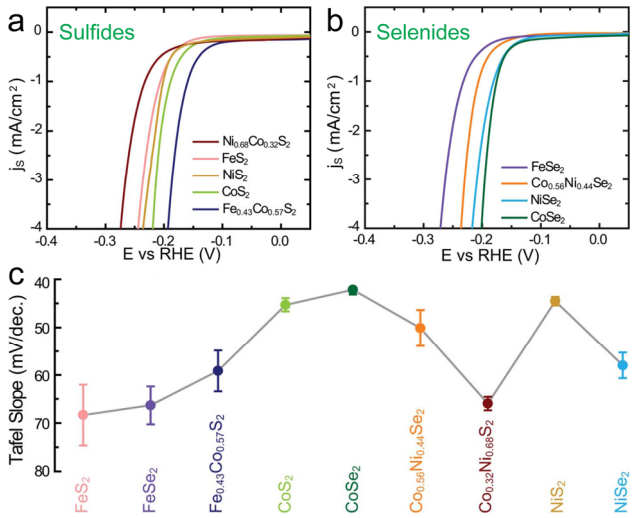

Fig. 8 Comparison of the performance of various pyrite-phase transition metal (a) disulfide and (b) diselenide HER electrocatalysts, along with (c) a comparison of their corresponding Tafel slopes. Adapted from Ref. 155 with permission from The Royal Society of Chemistry.

3.4.3. Amorphous materials. In the last few years, amorphous molybdenum sulfide (MoS_x, x = 2–3) has been identified as an effective electrocatalyst for the HER.[108,156] Despite lacking the well-defined catalytically active sites of MoS_2, amorphous MoS_x remarkably exhibits higher activity than as-synthesized crystalline MoS_2, achieving Tafel slopes as low as 40 mV decade^{-1} (Fig. 9).[156] Furthermore, amorphous MoS_x can be deposited on conducting substrates through facile and scalable electrodeposition[156-159] or wet chemical[160-162] syntheses at room temperature and atmospheric pressure, in contrast to the harsh conditions (high temperature, low pressure, *etc.*) typically employed to synthesize high-quality crystalline MoS_2, and reduced to the more active amorphous MoS_2 under standard electrochemical operating conditions. Amorphous MoS_x exhibits high HER activity and stability over a wide range of electrolyte acidities, making it compatible with most contemporary water-splitting and fuel cell technologies.[156] Recently it has been reported that codepositing amorphous MoS_x with conductive polypyrrole yields

composite electrocatalyst films with exceptional activity toward the HER.[158] Additionally, engineering strategies analogous to those employed for MoS_2 (and other earth-abundant inorganic electrocatalysts) have similarly been used to boost the HER electrocatalytic performance of amorphous MoS_x.[162,163]

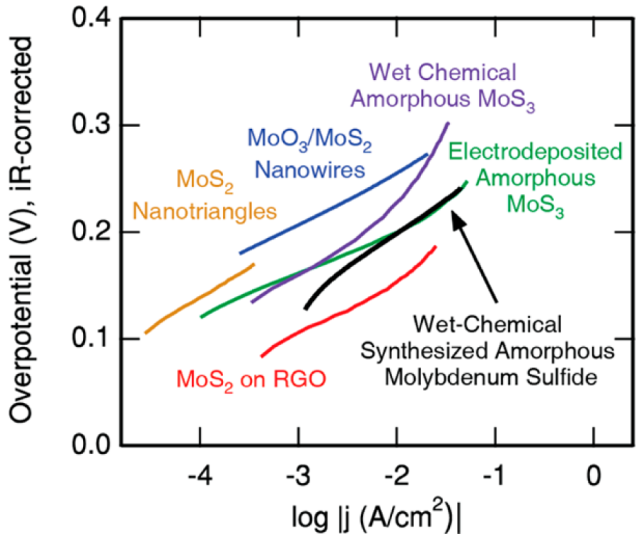

Fig. 9 Tafel plot comparing the intrinsic activity of various molybdenum sulfide electrocatalysts toward the HER. Adapted from Ref. 160 with permission from the American Chemical Society.

Following these reports of high electrocatalytic activity and previous demonstrations of MoS_2 as an effective cocatalyst for photocatalytic hydrogen evolution driven by visible light,[164] amorphous MoS_x has also been used to catalyze the photoelectrochemical splitting of water. When deposited over a Ti/TiO_x-protected n^+p-Si photocathode, amorphous MoS_x enables an onset of photoelectrochemical hydrogen evolution at 0.33 V vs. RHE, approaching that achieved when using platinum.[157] These photoelectrodes were relatively stable, with degradation in performance caused by failure of the Ti/TiO_x protection layer (resulting in surface oxidation of the photocathode) rather than the amorphous MoS_x electrocatalyst.[157] It was later found that Mo/MoS_2 can serve as a more chemically stable silicon protection layer than Ti/TiO_x, improving

long-term stability.[165] Amorphous MoS_x has also been electrochemically deposited over TiO_2-protected cuprous oxide (Cu_2O) photocathodes to enable photoelectrochemical hydrogen evolution.[159] The onsets of photocurrent for the MoS_x/n^+p-Si[157] and MoS_x/Cu_2O[159] photocathodes are more favorable than that for the 1T-MoS_2/*p*-Si heterojunction[127] due to a buried junction and more advantageous band bending; however, higher photocurrent density has been achieved using 1T-MoS_2/*p*-Si photocathodes, likely due to the high-quality semiconductor–electrocatalyst interface and the superior HER electrocatalytic activity of 1T-MoS_2. Recently, the use of amorphous transition metal chalcogenide electrocatalysts has expanded beyond just MoS_x, with amorphous cobalt sulfide (Co–S) films electrodeposited on conducting and semiconducting electrodes showing high activity toward electrochemical and photoelectrochemical hydrogen evolution in neutral or alkaline electrolytes.[166]

3.4.4. Other phases. A number of other transition metal chalcogenides and their nanostructures have emerged as promising electrocatalysts.[132] For example, sea urchin-like NiSe nanofiber assemblies exhibit HER activity comparable to supported MoS_2 electrocatalysts.[167] Additionally, CoS and Co_9S_8 have been shown to compete with platinum toward triiodide reduction in DSSCs.[168-170] Similarly, small-grain NiS films electrodeposited on FTO/glass show high electrocatalytic activity toward triiodide reduction and enable DSSC performance comparable to that achieved with conventional platinum counter electrodes.[171] Very recently, the metal selenides (including $Cu_{1.8}Se$ and PbSe) have emerged as a new class of efficient electrocatalysts for polysulfide reduction in QDSSCs.[172] Similarly, several transition metal selenides, including $Co_{0.85}Se$ and $Ni_{0.85}Se$, have also been shown to be efficient electrocatalysts for triiodide reduction in DSSCs.[173]

3.5. Transition metal nitrides.

As has also been the case for the transition metal sulfides, the use of transition metal nitrides as industrial catalysts, particularly for HDN,[60,174] inspired investigation of their applicability as electrocatalytic materials. Their stability in conditions of extreme pH and under high applied electrochemical bias makes them good candidate electrocatalyst materials.[39] Transition metal nitride compounds are commonly prepared by the thermal nitridation of transition metal-containing starting materials in the presence of ammonia.[39,175] Various transition metal nitrides have been examined as electrocatalyst materials, including the tungsten nitrides (WN and W_2N), molybdenum nitrides (MoN and Mo_2N), tantalum nitrides (TaN and Ta_3N_5), and nickel molybdenum nitrides ($NiMoN_x$), as well as titanium, vanadium, and niobium nitride (TiN, VN, and NbN, respectively).[175] Due to electronic modification of the transition metal *d*-band electron density of states, the transition metal nitrides are expected to exhibit enhanced noble metal-like activity toward those electrocatalytic transformations that involve the donation of *d* electrons, such as the HER.[174]

Noting the high activity of the Ni–Mo alloys toward the HER and the enhanced chemical stability of the transition metal nitrides over the corresponding metals, carbon-supported MoN and $NiMoN_x$ nanosheets were prepared and shown to exhibit improved HER activity and cycling stability in acidic conditions relative to carbon-supported spherical NiMo alloy nanoparticles.[176] The low Tafel slope of 35 mV $decade^{-1}$ exhibited by the $NiMoN_x$ nanosheets was rationalized by the high fraction of exposed active sites and a favorable catalytic synergism between nickel, which binds H weakly, and molybdenum, which binds H strongly.[72,176] Similarly, layered nanoparticulate cobalt molybdenum nitride ($Co_{0.6}Mo_{1.4}N_2$) has been reported as an efficient, stable HER electrocatalyst in both acidic and alkaline conditions with performance exceeding

that of the $NiMoN_x$ nanosheets.[177] The improved HER electrocatalytic activity of $Co_{0.6}Mo_{1.4}N_2$ and $NiMoN_x$ relative to their binary counterparts is illustrated in Fig. 10.

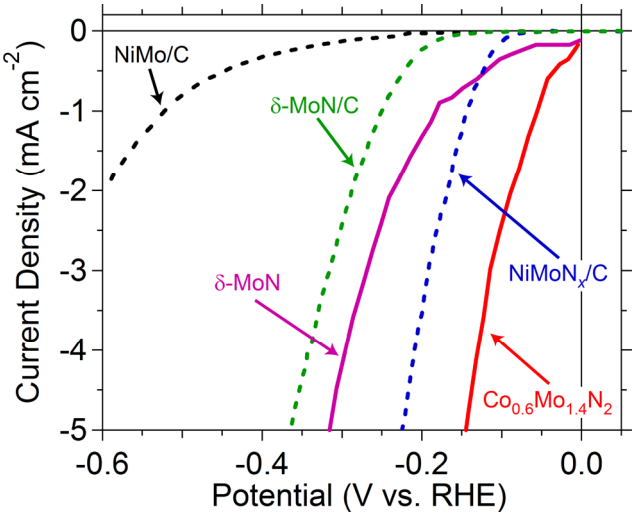

Fig. 10 Polarization curves illustrating the relative activity of carbon-supported NiMo nanoparticles (NiMo/C, black trace), *δ*-MoN nanosheets (*δ*-MoN/C, green trace), and NiMo nitride nanosheets ($NiMoN_x$/C, blue trace), as well as nanostructured MoN (*δ*-MoN, violet trace) and cobalt molybdenum nitride ($Co_{0.6}Mo_{1.4}N_2$, red trace) toward the HER in $H_2(g)$-saturated 0.1 M $HClO_4(aq)$. The dashed traces show the improved activity of the transition metal nitrides relative to the corresponding transition metal alloy catalyst, with the ternary $NiMoN_x$/C catalyst exhibiting superior performance. Similarly, the solid traces show that the electrocatalytic activity of nanostructured *δ*-MoN can be enhanced through the incorporation of Co and the concomitant formation of the $Co_{0.6}Mo_{1.4}N_2$ phase. Data for NiMo/C, *δ*-MoN/C, and $NiMoN_x$/C (dashed lines) obtained from Ref. 176; data for *δ*-MoN and $Co_{0.6}Mo_{1.4}N_2$ (solid lines) obtained from Ref. 177.

Transition metal nitrides have also been used for ORR electrocatalysis, with TiN nanocrystals prepared on nitrogen-doped graphene showing excellent activity.[178] Additionally, the high electrocatalytic activity of the transition metal nitrides has been noted in DSSCs, where

nanoparticulate MoN and WN counter electrodes enable DSSC performance approaching that of equivalent devices assembled with a platinum counter electrode.[179] The activity of TiN, VN, and MoN toward triiodide reduction is substantially enhanced when they are prepared as nanoparticles embedded in nitrogen-doped RGO, resulting in DSSC performance rivaling or even exceeding that achieved with a platinum counter electrode.[180] Similarly, the triiodide reduction performance of TiN–CNT composites greatly exceeds that of TiN nanoparticles alone due to the superior electrical conductivity of the CNT network (see additional discussion in Section 5.4).[181]

3.6. Transition metal phosphides.

Although the catalytic activity of transition metal phosphide compounds, such as dinickel phosphide (Ni_2P), has been known for over half a century,[182] they have only recently been investigated for heterogeneous (electro)catalysis.[60,183-185] In 1995, it was shown that the performance of electrodeposited amorphous Ni–P electrodes (*ca.* 3 wt% phosphorous content) toward the HER in alkaline conditions can be orders of magnitude higher than that of Ni electrodes.[186] Perhaps because such early works did not carry out detailed structural analysis of these transition metal phosphide materials (instead referring to them simply as "metal–phosphorous alloys"[187]), it was only very recently that the transition metal phosphides have reemerged as one of the most promising classes of earth-abundant inorganic electrocatalysts. Nanoporous iron monophosphide (FeP) nanosheets (Fig. 11a) prepared through an anion-exchange procedure exhibit an encouraging Tafel slope of 67 mV decade^{-1} toward the HER in 0.5 M H_2SO_4(*aq*), but their overall performance lags behind that of other earth-abundant HER electrocatalysts.[188] On the other hand, hollow and faceted Ni_2P nanoparticles (Fig. 11b) show HER activity and stability in 0.5 M H_2SO_4(*aq*) that is among the best for non-noble

electrocatalysts.[189] More recently, cobalt phosphide (CoP) nanoparticles[190] (Fig. 11c), nanoporous nanowire arrays[191] (Fig. 11d), nanosheets,[192] and nanoparticles on CNTs[193] have been reported to exhibit both superb activity toward the HER and long-term stability in acidic conditions, with some morphologies surpassing the performance of nanostructured Ni_2P. To highlight the recent rapid advances in transition metal phosphide HER electrocatalyst performance, the polarization data for the FeP nanosheet, Ni_2P nanoparticle, CoP nanoparticle, and CoP nanowire electrodes have been compared in Fig. 11e. More recently, the HER activities of various molybdenum phosphides were compared to show that the extent of metal phosphorization can affect both activity and stability.[194]

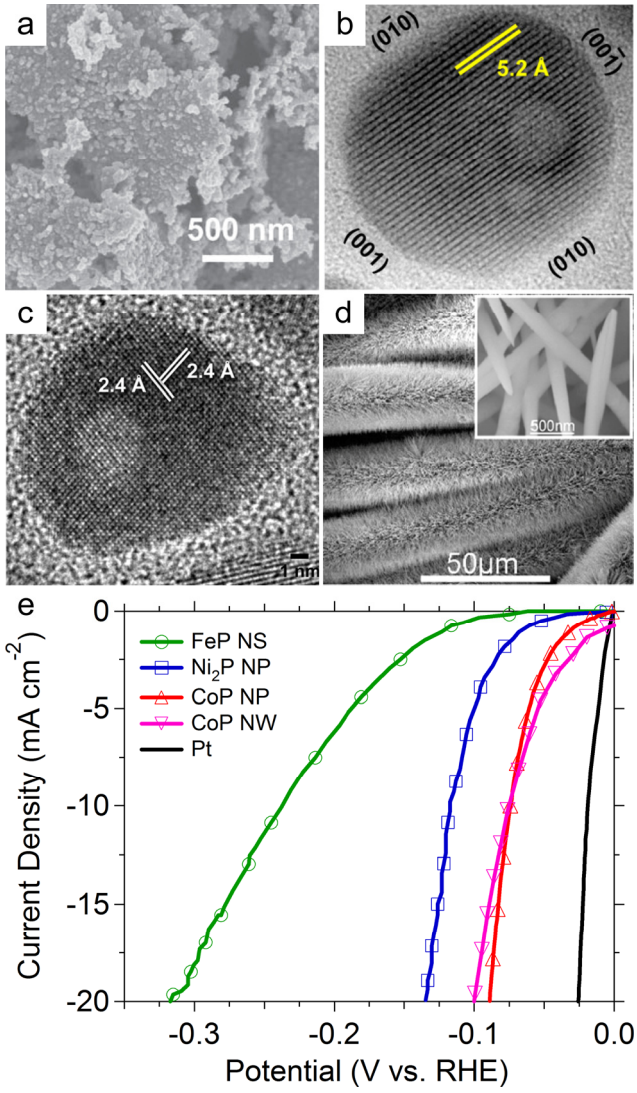

Fig. 11 Electron microscopy characterization of (a) iron phoshide (FeP) nanosheets (NS), (b) nickel phosphide (Ni_2P) nanoparticles (NP), (c) cobalt phosphide (CoP) NP, and (d) CoP nanowires (NW) supported by carbon cloth, along with (e) polarization curves comparing their electrocatalytic activity toward the HER in 0.5 M H_2SO_4(*aq*) electrolyte in comparison with that of a Pt standard (black trace). Images and data for the FeP NS, Ni_2P NP, and CoP NW electrodes obtained from Refs. 188 (with permission from The Royal Society of Chemistry), 189, and 191 (both with permission from The American Chemical Society), respectively. Image and data for

the CoP NP and Pt standard electrodes obtained from Ref. 190 with permission from Wiley-VCH Verlag GmbH & Co. KGaA.

Besides the HER, there has also been recent interest in the use of transition metal phosphides as electrocatalysts in DSSCs.[53] For example, nickel phosphide ($Ni_{12}P_5$) has been reported as an effective triiodide reduction electrocatalyst.[195] Embedding $Ni_{12}P_5$ in graphene resulted in a synergistic enhancement of DSSC performance, with overall conversion efficiency approaching that of equivalent devices assembled with a platinum/FTO counter electrode.[195] The Ni_5P_4 phase of nickel phosphide and molybdenum phosphide (MoP) have also been demonstrated as counter electrode electrocatalysts in DSSCs, with the performance of Ni_5P_4 exceeding that of MoP.[196] As is also the case for $Ni_{12}P_5$, the preparation of Ni_5P_4 as a composite with mesoporous carbon boosts its performance nearly to the level of platinum-based counter electrodes.[196]

3.7. Transition metal carbides.

Since the observation by Levy and Boudart that tungsten carbide can exhibit platinum-like behavior,[197] the catalytic activity[198] and surface properties[174,199] of many transition metal carbides have been studied in great detail. Recently, the platinum-like properties of the transition metal carbides have inspired research into their use as replacements for noble metal electrocatalysts in energy conversion applications, particularly for the HER.[175] Along with the transition metal nitrides, the transition metal carbides share the desirable attributes of corrosion resistance, stability, and mechanical strength, suggesting long electrocatalyst lifetime.[175] Tungsten monocarbide (WC) is the most widely studied transition metal carbide for electrocatalysis, due to its high activity, high electrical conductivity, and low sensitivity to the

molecular compounds that can poison noble-metal electrocatalysts, such as hydrogen sulfide and carbon monoxide, making it particularly attractive for fuel cell applications.[39,175] Furthermore, increased resistance to surface oxidation at low pH as compared to more metal-rich carbides (*e.g.*, W_2C or Mo_2C) means that WC is a more suitable HER electrocatalyst in acidic conditions.[200] Besides WC, many other transition metal carbides have been studied as electrocatalysts for the HER. Bulk Mo_2C has been shown to be an active HER electrocatalyst in both acidic and alkaline environments, achieving Tafel slopes as low as 54 mV decade^{-1}.[201] Nanoporous Mo_2C nanowires show improved HER performance in acidic electrolyte due to increased surface area and diffusion of species through the open structures.[202,203] It was recently demonstrated that Mo_2C nanoparticles prepared on carbon nanotubes show vastly improved activity toward the HER as compared to bulk Mo_2C or Mo_2C on a carbon black support, mostly due to favorable electronic interactions between the Mo_2C nanoparticles and the CNT support.[204] Furthermore, nanoparticles of other molybdenum carbide phases, including α-MoC_{1-x}, η-MoC, and γ-MoC, have been synthesized and shown to exhibit encouraging stability and activity toward the HER.[205]

Noting their high activity toward electrocatalytic water splitting, transition metal carbide electrocatalysts have also been used for solar energy conversion.[53] For example, tungsten semicarbide (W_2C) thin films deposited on *p*-type silicon photoelectrodes have been reported as effective catalysts for the photoelectrochemical evolution of hydrogen.[206] In addition, composite counter electrodes consisting of MoC, Mo_2C, or WC particles embedded in ordered mesoporous carbon (or other conductive additives) achieve conversion efficiencies in DSSCs employing the iodide/triiodide redox electrolyte rivaling or even exceeding that of devices assembled with a platinum counter electrode.[207] Noting the importance of high surface area to achieving high

device performance, mesoporous WC films prepared on FTO/glass have been shown to serve as effective counter electrodes for DSSCs, achieving 85% of the solar light-to-electricity power conversion efficiency that can be achieved with platinum counter electrodes in equivalent devices.[208] Similarly, various transition metal carbides have been investigated as electrocatalytic electrode materials for a variety of redox couples used in liquid-junction QDSSCs. Titanium carbide (TiC) electrodes prepared through a spray-coating method enable performance rivaling that of platinum counter electrodes in tin sulfide (SnS)-sensitized QDSSCs that employ either the iodide/triiodide, disulfide/thiolate, or sulfide/polysulfide redox couple.[209] Similarly, the performance of TiC counter electrodes in cadmium sulfide (CdS)-sensitized QDSSCs filled with the sulfide/polysulfide redox electrolyte has also been shown to exceed that of gold counter electrodes.[210]

3.8. Transition metal silicides.

The transition metal silicides represent a relatively underexplored class of potential earth-abundant inorganic electrocatalysts, and, in general, their usage in catalysis has been limited. Following computational work suggesting high hydrogen sulfide tolerance for the metal silicides,[211] several first-row transition metal silicides have been investigated as HDS catalysts.[212,213] Analogous transition metal silicides have also been explored as carbon monoxide methanation catalysts.[214] However, despite most transition metal silicides possessing high electrical conductivity and good electrochemical stability, there have been few studies of their electrocatalytic activity. That said, several transition metal silicides have been previously investigated as electrocatalysts for the HER in both acidic[215] and alkaline[216] conditions, with the emerging trends in activity suggesting possible pathways toward improved silicide electrocatalysts.[217] While the performance of the earth-abundant transition metal silicides falls

far behind that of silicides containing noble metals,[217] the promising HER activity of certain earth-abundant transition metal silicides (VSi_2, Cr_3Si, FeSi, $CoSi_2$, $NiSi_2$, and Cu_5Si, among others) encourages further exploration. Indeed, even commercial molybdenum silicide ($MoSi_2$) and tungsten silicide (WSi_2) powders were recently shown to exhibit decent HER electrocatalytic activity and stability in 0.1 M $H_2SO_4(aq)$.[218] Moreover, as a rich family of materials with an ever-increasing number of controlled synthesis strategies for obtaining unique morphologies, including nanowires,[219] nanoparticles,[220] and high surface area hierarchical structures,[221] there are likely other transition metal silicides (and related intermetallic compounds) that could serve as effective earth-abundant electrocatalysts, yet remain to be investigated.

3.9. Transition metal borides.

Like the transition metal phosphides, the transition metal borides represent a family of materials with known catalytic activity whose members have seldom been explored as electrocatalysts for energy conversion applications.[60,185] For electrocatalytic applications, the superior electrical conductivity (often higher than the parent metal itself) and anticipated chemical inertness of the transition metal borides make them especially attractive.[185] Although crystalline metal-rich borides such as Ni_3B and Co_2B were found to be susceptible to sulfidation when exposed to the high temperatures of industrial HDS, amorphous transition metal borides (often loosely referred to as "metal–boron alloys," as in the case of the amorphous transition metal phosphides) show enhanced stability and activity.[60,185] Various amorphous transition metal borides (and alloys thereof) can be prepared as supported and unsupported particles through the facile reaction of metal halide and borohydride salt solutions.[60,187] For example, both undoped[222] and doped[223] amorphous nickel boride (Ni_2B) have been explored as HER electrocatalysts in alkaline electrolytes. Recently, molybdenum boride (MoB) was shown to catalyze the HER in

both acidic and alkaline conditions with reasonable efficiency, but it experienced rapid corrosion at pH 14.[201] At pH 0, however, the MoB catalyst was stable over long periods of continuous operation.[201] Although surface oxides rapidly form when MoB is exposed to air, these oxides can be cathodically removed under normal HER operating conditions.[201] Commercial titanium boride (TiB_2), tungsten boride (WB), and zirconium boride (ZrB_2) powders have also been demonstrated as HER electrocatalysts in 0.1 M $H_2SO_4(aq)$, though their performance was modest and their rates of corrosion were relatively high.[218]

3.10. Transition metal compound alloys and mixed-anion compounds.

Given the wide range of binary transition metal compounds that exhibit electrocatalytic activity toward redox processes central to energy conversion, and the fact that the activity of several electrocatalysts can be enhanced by mixing multiple transition metals, it is reasonable to expect that more complex transition metal compounds or compound alloys might possess further enhanced electrocatalytic activity. As has been demonstrated for the transition metal alloy electrocatalysts, the controlled introduction of additional cations (or anions) to a host compound is expected to modify its electrocatalytic activity due to changes in its electronic properties and/or the geometric arrangement of atoms. This concept has been perhaps best exemplified in the nitride system, where the ternary $NiMoN_x$ and $Co_{0.6}Mo_{1.4}N_2$ compounds exhibit significantly higher activity than δ-MoN, perhaps owing to favorable interactions between metal atoms (Fig. 10). Similarly, other relevant properties, such as chemical stability, could also be altered through changes in composition. Many mixed-anion transition metal compounds, such as oxynitrides and carbonitrides, have been investigated as electrocatalysts, particularly for the ORR.[39] In addition, carbon- and nitrogen-containing "N–M–C" (M = Co and/or Fe) electrocatalysts derived from polyaniline, although not strictly of a well-defined carbonitride phase, have been shown to

exhibit superb activity, long-term stability, and four-electron selectivity toward the ORR (*i.e.*, low hydrogen peroxide yield).[224] Carbonitride compounds have been scarcely explored as HER electrocatalysts, but tungsten carbonitride (WCN) with a high fraction of tungsten nitride (WN) shows decent activity and high stability in both acidic and alkaline media.[225]

4. Challenges facing earth-abundant inorganic electrocatalysts

For earth-abundant inorganic electrocatalysts to become competitive with those containing noble metals, there are a number of specific challenges that must be overcome. Most obvious among these is the desire for comparable (or as nearly comparable as possible) levels of intrinsic electrocatalytic activity. While various strategies might be employed to boost the performance of electrocatalysts with inferior intrinsic activity, materials with higher intrinsic activity will always be preferred. Indeed, when examining a new potential electrocatalyst, its intrinsic activity toward the electrochemical process of interest is usually the first property probed, as low activity can immediately render a candidate material uninteresting. Second, the electrocatalyst must be sufficiently stable in the conditions of electrocatalysis to permit long-term usage without performance decay. Typically, electrocatalyst stability is reported under continuous operating conditions. However, in such tests, the electrical bias applied to drive catalysis might suppress electrocatalyst corrosion (*e.g.*, oxidation). Ideally, earth-abundant electrocatalysts should also be highly stable under "standby" (or "shutdown") conditions, where no bias is applied, or even under conditions of current reversal. While the strict requirements for long-term stability might be relaxed somewhat for earth-abundant electrocatalysts that can be

easily replaced or regenerated, the ideal materials should be sufficiently stable as to permit indefinite operation with minimal decay in performance.

Various secondary requirements should also be met by ideal earth-abundant electrocatalysts, including superior electrical conductivity, chemical compatibility, and catalytic generality. Metallically conducting electrocatalysts ensure fast charge carrier transport and minimal electrode polarization (*i.e.*, low Ohmic losses) under operating conditions and, hence, maximum efficiency. Electrocatalytic activity (in the form of a Tafel slope) is often reported and compared after *IR* correction to ensure a fair comparison of intrinsic activity between candidate materials, particularly over regions of low to modest current densities. However, such a comparison ignores the benefits of low overall series resistance in enabling high current densities at reduced overpotentials, which is especially relevant in practical water electrolysis systems. Earth-abundant electrocatalysts should also possess high chemical compatibility with their operating environment, such that they are not poisoned during operation, nor should they contaminate or degrade other components of the electrochemical system. This requirement is particularly relevant for electrocatalysts used at the counter electrodes of photoelectrochemical solar cells, since they must maintain stable performance in the presence of the redox electrolyte while also not contaminating or otherwise altering the behavior of the light-absorbing photoelectrode. Lastly, the ideal earth-abundant electrocatalyst should be widely applicable, exhibiting high activity toward many catalytic processes while still remaining highly selective in their respective environments. Much like the many electrocatalytic roles of the noble metals and compounds thereof, earth-abundant alternatives with sufficiently high activity and stability would optimally catalyze a range of diverse redox reactions, thereby eliminating the need to develop new and unique earth-abundant electrocatalysts for each redox system of interest.

5. Strategies for enhancing earth-abundant inorganic electrocatalyst performance and stability

Many chemical and engineering strategies have been shown to boost the performance and stability of earth-abundant inorganic electrocatalysts. These efforts are aimed at increasing the activity of the electrocatalyst toward the redox process of interest, the number of available sites for catalysis, or in some cases, both. Maximizing these two factors ensures that the electrocatalyst operates at the highest possible level of performance. Most earth-abundant inorganic electrocatalysts offer opportunities to enhance their performance by addressing one or both of these factors either synthetically or through post-synthetic treatments. Here, we will outline the commonly demonstrated strategies for increasing electrocatalyst performance, pointing out key examples of each.

5.1. Nanostructuring.

It is well known that the magnitude of an electrocatalytic current will scale with the effective surface area of the electrocatalyst.[32] While modification to the chemical composition or structural phase of the electrocatalyst might increase the areal density of active sites for catalysis, morphological changes, such as nanostructuring, that increase the real surface area could also increase the number of available active sites. Without changing the per site turnover frequency, simply multiplying the number of available sites through an increase in surface rugosity will necessarily enhance the overall electrocatalytic performance. This is perhaps the most straightforward—and commonly utilized—strategy for increasing electrocatalyst performance.

One early recognition of the role of real surface area in promoting the overall performance of an earth-abundant electrocatalyst was in the transition metal alloy system, where researchers noted that the surface roughness of alloy catalysts was commonly higher than that of pure metal systems, affording more available sites for catalysis.[76] This phenomenon was particularly relevant for the Ni–Mo alloy HER electrocatalysts, where the electrode surface rugosity was further increased by selective leaching of molybdenum.[29,76,78,82] By preparing the Ni–Mo material in a nanoparticulate morphology,[79] the real surface area (and, consequently, electrocatalytic performance) could be further increased. Similarly, nanomaterial synthesis strategies ranging from templated preparations to spontaneous solution- or gas-phase growth have been applied in most of the classes of earth-abundant inorganic electrocatalysts detailed in Section 3 in order to increase their electrocatalytic performance. Additionally, post-synthetic strategies for increasing real surface area, such as the chemical exfoliation of the layered TMD materials MoS_2[116] and WS_2[51,117] through a lithium intercalation treatment, have been shown to be effective in increasing electrocatalytically active surface area (Fig. 5).

The role of electrocatalyst nanostructuring in improving electrocatalytic performance has been clearly demonstrated through the comparison of CoS_2 film, microwire, and nanowire electrode activity toward the HER.[50] Despite similar synthetic procedures for arriving at the different CoS_2 morphologies, thus leading to a consistent intrinsic activity and areal density of active sites, they exhibit vastly different levels of overall electrocatalytic performance (with the CoS_2 nanowire electrodes enabling the highest performance) owing to their different electrochemical surface areas (Fig. 7).[50] In this example, the relative effective electrochemical surface areas were determined by measuring the electrode double-layer capacitance,[49,50] which is proportional to the surface area. The generality of the nanostructuring strategy was also

demonstrated by the improved performance of CoS_2 nanowire electrodes toward polysulfide and triiodide reduction as compared to CoS_2 film electrodes.[50] Furthermore, this work establishes that, in the electrocatalysis of gas-evolving applications such as water splitting, electrocatalysts with a micro- or nanowire morphology can effectively promote gas bubble release from the electrode surface (Fig. 7c), simultaneously enabling high current densities at reduced overpotentials and dramatically improved electrode stability.[50]

The many demonstrations of improved electrocatalyst performance through nanostructuring motivate the preparation of earth-abundant inorganic electrocatalysts in nanoscale morphologies. With the growing number of strategies for the controlled synthesis of nanomaterials,[132,134,185,219,226,227] the opportunities for preparing earth-abundant electrocatalysts in morphologies that maximize both the fraction of exposed active sites and the long-term operational stability of the materials similarly grow. In cases where the active sites for catalysis are known and well-characterized, controlled nanomaterials synthesis could afford the opportunity to prepare the inorganic electrocatalyst material with predominant exposure of those most active facets. Similarly, high surface area electrocatalyst supports, such as conductive nanowire arrays, hierarchical structures,[226] or mesoporous film scaffolds,[163] could be employed to further enhance the real electrocatalyst surface area. It may also be the case that the intrinsic activity of a nanostructured electrocatalyst material differs from that of its bulk counterpart, perhaps due to variations in surface composition, atomic arrangement, or electronic properties at the nanoscale, further motivating their controlled synthesis and characterization.

5.2. Chemical modification.

The trends in the electrocatalytic activity of the transition metals and transition metal alloys clearly establish that the electronic structures and properties of electrocatalysts play a key role in determining their activity. Similarly, the effects of "promoter" species in increasing the intrinsic activity of certain electrocatalysts has been documented.[112] Drawing on the wealth of established knowledge regarding the doping of semiconductor materials to alter their electronic properties, one could imagine incorporating "dopant" or "promoter" species into established earth-abundant electrocatalysts to enhance their activity. By including either electron-poor or electron-rich species into a host material, it may be possible to tune its Fermi level and other electrical properties for enhanced electrocatalytic activity. These "dopant" species may also alter the oxidation state of the catalytic centers, modifying their intrinsic activity. This concept has been more systematically explored through the investigation of transition metal alloys and, to a lesser extent, transition metal compound alloys (see discussion in Sections 3.2 and 3.10, respectively), but the controlled preparation and physical property characterization of other candidate materials could enable a more direct route toward high-performance earth-abundant electrocatalysts.

5.3. Structural modification.

In addition to chemical modification, changes in atomic arrangement may modify the physical properties of a material to improve its electrocatalytic activity. For example, the chemical exfoliation of MoS_2 and WS_2, as discussed in Section 3.4.1, has been noted to increase surface area and proliferate the density of catalytic edge sites.[51,116,117] More importantly, though, this lithium intercalation and exfoliation treatment induces a phase transformation from the thermodynamically-favored semiconducting 2H polymorph to the metallically conducting 1T polymorph (Fig. 5a), which exhibits enhanced HER activity (Fig. 5f–g). The transfer of an

electron upon lithium intercalation destabilizes the trigonal prismatic 2H-MX_2 structure and instead favors the metastable octahedrally coordinated 1T polymorph.[228] The reduced Tafel slope of 1T-MoS_2 (Fig. 5f, inset) indicates that this phase transformation improves its intrinsic electrocatalytic activity through a modification of electronic properties. In other words, the semiconducting 2H layered TMDs become intrinsically better electrocatalysts once converted to their corresponding 1T polymorph. This is the most important benefit of the chemical exfoliation treatment. To a certain degree, then, chemical modification/electronic structure tuning (see Section 5.2) and structural modification may be interconnected strategies. The increase in electrocatalytic activity that accompanies the 2H to 1T transition has also been continuously tuned electrochemically and monitored using vertically aligned MoS_2 nanofilms.[119] The metallically conducting nature of the 1T polymorph also reduces Ohmic losses as compared to the 2H polymorph, further enhancing electrocatalytic performance. These benefits should also translate to improved performance in other electrocatalytic processes, such as triiodide or polysulfide reduction. While in other families of earth-abundant inorganic electrocatalysts the differences in activity between structural polymorphs mostly remain to be investigated, the case of MoS_2 serves to illustrate that the particular crystal structure and bonding environment around catalytically active sites should be carefully considered and, where possible, modified to achieve maximum activity.

Moreover, modifications of crystalline structure at the atomic level (through, for example, the creation of lattice defects or interstitial species, grain boundaries, or dislocations) might produce sites with new or altered electrocatalytic activity.[120,121] Similarly, the recent success of amorphous HER electrocatalysts has renewed interest in studying the activity of materials that lack a well-defined crystal structure. The absence of long-range order in

amorphous materials suggests that there might be new or unusual bonding arrangements (or a specific rate of occurrence thereof) that are favorable for electrocatalysis. Additionally, amorphous materials are expected to have a greater density of dangling bonds that could modify their affinity for adsorbates and, therefore, their electrocatalytic activity. Such concepts have been proposed to explain the electrocatalytic activity of amorphous transition metal alloys,[82] transition metal sulfides (particularly MoS_x),[108,156-161] Ni–P compounds,[186,187] and Ni–B compounds.[60,185,187] The precise origin of electrocatalytic activity in these amorphous materials is not fully resolved, but reports suggest the possibility of catalytic domains embedded in an amorphous matrix.[60,160] The specific oxidation state of catalytic centers (or the fact that a dispersion of oxidation states may simultaneously exist) in these amorphous electrocatalysts could also contribute to their elevated activity. Interestingly, the impressive performance of these amorphous electrocatalysts suggests that, in some instances, a well-defined crystal structure may be unnecessary—or even deleterious—in achieving high activity. Of course, the general challenge in studying amorphous electrocatalysts is the difficulty in elucidating their structural details using common materials characterization techniques (*e.g.*, X-ray and electron diffraction, electron microscopy, or infrared and Raman spectroscopy). However, we need to better understand their atomic structures using new techniques in order to advance these materials, because it is likely that under the general description of "amorphous materials" there are many subtle structural differences that may impact catalytic activity.

5.4. Composite materials.

The performance of high-activity electrocatalysts—particularly those with poor electrical conductivity—can be enhanced through the preparation of a composite containing a conductive additive, such as carbon black, carbon nanofibers or microfibers, graphene, RGO, CNTs, or

polymers. Integration of the electrocatalyst material with a conducting support typically leads to improvements in both performance and stability, since directly anchoring the electrocatalyst to a robust conducting support ensures a low-resistance electrical transport pathway as well as reduced likelihood of physical delamination of the electrocatalyst. Electronic coupling between the support and catalyst materials can synergistically boost intrinsic activity as well.[90,91,115,178,204,229,230] As an example, these effects have been clearly demonstrated for MoS_2 nanoparticles synthesized directly on RGO sheets (Fig. 12a), which exhibit markedly enhanced intrinsic electrocatalytic activity and performance toward the HER as compared to unsupported MoS_2 particles (Fig. 12b).[115] Similarly, amorphous MoS_x layers directly bound to vertically-aligned N-doped CNTs (Fig. 12c) expose a particularly high density of catalytic sites and benefit from the excellent charge transport properties of the N-doped CNT supports, leading to electrocatalytic activity toward the HER approaching that of a commercial carbon-supported platinum electrocatalyst (Fig. 12d).[162]

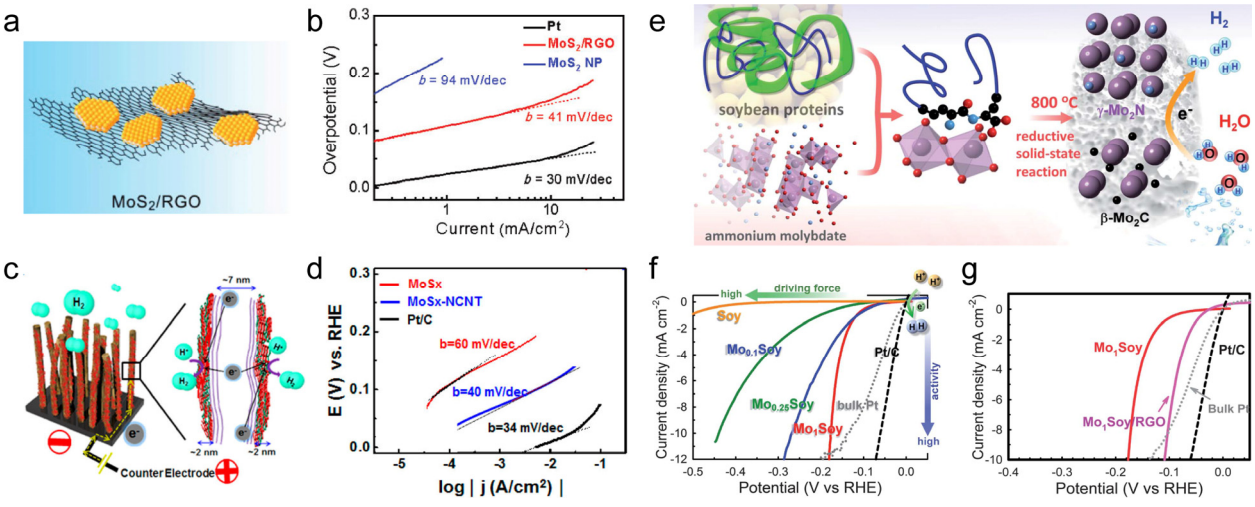

Fig. 12 Schematic illustrations and performance characterizations of MoS_2/RGO, MoS_x/N-doped CNT, and biomass-derived "MoSoy" composite HER electrocatalysts. (a) MoS_2

nanoparticles synthesized directly on RGO sheets, which (b) exhibit dramatically increased electrocatalytic activity as compared to unsupported MoS_2 particles. (c) Amorphous MoS_x layers prepared directly on a N-doped CNT array, with (d) intrinsic electrocatalytic activity approaching that of a commercial Pt/C electrocatalyst. (e) Schematic illustration of the preparation of the "MoSoy" composite electrocatalyst, which contains both crystalline β-Mo_2C and γ-Mo_2N domains. (f) The HER electrocatalytic performance of the "MoSoy" composite varies with Mo content, with the "Mo_1Soy" composite (prepared using a 1:1 ratio of Mo precursor to soybean powder) exhibiting the highest performance. (g) The HER electrocatalytic performance of the "MoSoy" electrocatalyst can be significantly improved through preparation on a RGO conductive support. Panels a and b adapted from Ref. 115, and panels c and d adapted from Ref. 162, both with permission from the American Chemical Society; panels e–g adapted from Ref. 231 with permission from The Royal Society of Chemistry.

Electrocatalytic composites can also be prepared for the purpose of increasing robustness and long-term stability. One interesting example is the biomass-derived "MoSoy" catalyst synthesized through the solid-state reaction of ammonium molybdate with soybean powder (Fig. 12e).[231] The resultant "MoSoy" composite consists of catalytic β-Mo_2C nanoparticles and acid-stable γ-Mo_2N nanoparticles embedded in amorphous carbon, which serves to increase the overall surface area of the composite.[231] The "MoSoy" electrocatalyst deposited on a carbon fiber paper support exhibits good activity toward the HER in 0.1 M $HClO_4$(*aq*), with its performance increasing with Mo content (Fig. 12f). This activity can be further increased by preparing the "MoSoy" material directly on a RGO support (Fig. 12g), resulting in electrocatalytic performance competitive with the best earth-abundant HER electrocatalysts. Most importantly, the presence of the acid-stable γ-Mo_2N phase increases the long-term stability

of the "MoSoy" electrocatalyst under operating conditions as compared to carbon black-supported β-Mo_2C nanoparticles. This example demonstrates that composite electrocatalysts containing catalytically active domains and domains with high chemical stability can synergistically benefit from both.

6. Summary and perspectives

In this review, we have summarized recent advances in the development of earth-abundant inorganic heterogeneous electrocatalysts for energy conversion applications by examining families of materials classified by their elemental compositions. The discussion of electrocatalysis has focused on the cathodic reactions where there are clear opportunities for earth-abundant electrocatalysts, namely, the hydrogen reduction reaction, the oxygen reduction reaction, and the redox reactions in regenerative liquid-junction photoelectrochemical cells. We have also discussed the key challenges facing such earth-abundant electrocatalysts, and enumerated several current and emerging strategies for improving their performance, including nanostructuring, chemical modification, structural modification, and the preparation of composite materials.

The field of electrocatalysis is undergoing rapid expansion, both in terms of new materials being explored and new applications being developed. The recent emergence (or reemergence) of earth-abundant materials with known catalytic activity (toward, for example, the HDS or HDN reactions) as inorganic electrocatalysts for energy conversion suggests that particular attention should be paid to those catalysts carefully studied and developed for industrial applications. The similarity of certain electrochemical redox processes (such as HER)

to those catalyzed with high efficiency in industrial chemical refining warrants further attention and suggests potential repurposing of these materials for electrocatalysis. Likewise, chemical or structural analogues of known high-performance (electro)catalysts could exhibit comparable (or even improved) activity and should therefore be explored. The study and development of catalytic materials stretching back several decades offers a wealth of knowledge to scientists seeking to develop earth-abundant electrocatalysts for energy conversion applications, which certainly should be leveraged. At the same time, the recent explosion in the number and variety of earth-abundant inorganic electrocatalysts suggests that we should expand even further into the periodic table, investigating new and increasingly complex materials that might enable more finely tuned electrocatalytic activity, perhaps beginning with the ternary compounds and alloys. The use of combinatorial techniques for screening new catalyst compositions appears to be a very promising and effective approach, especially for compounds with complex stoichiometries.[153,232-235]

Until now, the discovery of earth-abundant inorganic electrocatalysts has remained largely Edisonian. Despite a recent uptick in theoretical and computational studies aimed at predicting promising candidates,[54,57,58,110] few emergent high-performance earth-abundant electrocatalysts have been rationally designed at a chemical and/or structural level based on the mechanism of the chemical transformation of interest. Instead, most recent reports of "new" earth-abundant electrocatalysts have focused on the controlled synthesis of materials (some with well-known catalytic activity) and characterization of their electrocatalytic activity and long-term stability, with little attention paid to the origin or fundamental nature of their activity. While such an approach certainly serves to advance the field in a practical sense, the lack of a basic understanding of such electrocatalytic activity could retard more directed and rational earth-

abundant inorganic electrocatalyst development. As illustrated here, various classes of earth-abundant electrocatalysts are under rapid simultaneous screening, but *a priori* knowledge of the mechanism of catalysis and the relevant physical properties of potential earth-abundant electrocatalysts might enable more informed, in-depth studies of the most promising candidates, accelerating the rate of discovery and advance.

The progress of molybdenum sulfide-based electrocatalysts for the HER perhaps best illustrates how earth-abundant electrocatalyst development could proceed most efficiently. In this case, fundamental mechanistic studies of molecular systems,[65,113] supported by theory,[110] led to the identification of MoS_2 as a potential inorganic analogue. Then, careful analytical studies identified the edges of MoS_2 as being most active sites for HER electrocatalysis,[111] and understanding of its layered structure inspired the study of well-defined molecular mimics that confirmed this edge-site activity.[113,152] With this knowledge, various synthetic and engineering strategies were employed to maximize the exposure of these edge sites, improving the HER electrocatalytic performance of MoS_2. Modification of the intrinsic activity and electrical transport properties of MoS_2 through a phase transformation has further increased its activity.[116] At the same time, MoS_2-based composite electrocatalysts have been prepared and shown to exhibit activities beyond those achieved with MoS_2 alone.[115] Still, unexpected discoveries, such as the high electrocatalytic activity of the amorphous molybdenum sulfides,[156] occurred along this path of development, but the combined efforts of theorists and experimentalists clearly helped to establish a roadmap for the development of high-performance MoS_2-based electrocatalysts. Only through a balanced combination of theoretical, fundamental, and performance-based studies will the development of earth-abundant inorganic electrocatalysts for energy conversion progress at the rapid rate necessary to address our growing energy demand.

Acknowledgments

This research is supported by the U.S. Department of Energy, Office of Basic Energy Sciences, Division of Materials Sciences and Engineering, under Award DE-FG02-09ER46664. M.S.F. acknowledges support from the National Science Foundation Graduate Research Fellowship Program. S.J. thanks the Research Corporation for Science Advancement Scialog Award for Solar Energy Conversion and the UW–Madison H. I. Romnes Faculty Fellowship for support.

References

1 N. S. Lewis and D. G. Nocera, *Proc. Natl. Acad. Sci. U.S.A.*, 2006, **103**, 15729–15735.

2 T. Saga, *NPG Asia Mater.*, 2010, **2**, 96–102.

3 M. Grätzel, *Nature*, 2001, **414**, 338–344.

4 Best Research-Cell Efficiencies, http://www.nrel.gov/ncpv/images/efficiency_chart.jpg, (accessed June 2014).

5 N. S. Lewis, *Science*, 2007, **315**, 798–801.

6 C. A. Wolden, J. Kurtin, J. B. Baxter, I. Repins, S. E. Shaheen, J. T. Torvik, A. A. Rockett, V. M. Fthenakis and E. S. Aydil, *J. Vac. Sci. Technol. A*, 2011, **29**, 030801.

7 M. Graetzel, R. A. J. Janssen, D. B. Mitzi and E. H. Sargent, *Nature*, 2012, **488**, 304–312.

8 A. Hagfeldt, G. Boschloo, L. C. Sun, L. Kloo and H. Pettersson, *Chem. Rev.*, 2010, **110**, 6595–6663.

9 S. Rühle, M. Shalom and A. Zaban, *ChemPhysChem*, 2010, **11**, 2290–2304.

10 P. V. Kamat, *J. Phys. Chem. Lett.*, 2013, **4**, 908–918.

11 R. S. Selinsky, Q. Ding, M. S. Faber, J. C. Wright and S. Jin, *Chem. Soc. Rev.*, 2013, **42**, 2963–2985.

12 E. H. Sargent, *Nature Photon.*, 2012, **6**, 133–135.

13 J. Nelson, *Mater. Today*, 2011, **14**, 462–470.

14 T. Todorov and D. B. Mitzi, *Eur. J. Inorg. Chem.*, 2010, 17–28.

15 H. J. Snaith, *J. Phys. Chem. Lett.*, 2013, **4**, 3623–3630.

16 P. P. Boix, K. Nonomura, N. Mathews and S. G. Mhaisalkar, *Mater. Today*, 2014, **17**, 16–23.

17 J. R. Szczech and S. Jin, *Energy Environ. Sci.*, 2011, **4**, 56–72.

18 J. B. Goodenough and Y. Kim, *Chem. Mater.*, 2010, **22**, 587–603.

19 T. R. Cook, D. K. Dogutan, S. Y. Reece, Y. Surendranath, T. S. Teets and D. G. Nocera, *Chem. Rev.*, 2010, **110**, 6474–6502.

20 J. A. Turner, *Science*, 2004, **305**, 972–974.

21 X. B. Chen, S. H. Shen, L. J. Guo and S. S. Mao, *Chem. Rev.*, 2010, **110**, 6503–6570.

22 J. R. McKone, N. S. Lewis and H. B. Gray, *Chem. Mater.*, 2014, **26**, 407–414.

23 E. E. Benson, C. P. Kubiak, A. J. Sathrum and J. M. Smieja, *Chem. Soc. Rev.*, 2009, **38**, 89–99.

24 S. C. Roy, O. K. Varghese, M. Paulose and C. A. Grimes, *ACS Nano*, 2010, **4**, 1259–1278.

25 A. M. Appel, J. E. Bercaw, A. B. Bocarsly, H. Dobbek, D. L. DuBois, M. Dupuis, J. G. Ferry, E. Fujita, R. Hille, P. J. A. Kenis, C. A. Kerfeld, R. H. Morris, C. H. F. Peden, A.

R. Portis, S. W. Ragsdale, T. B. Rauchfuss, J. N. H. Reek, L. C. Seefeldt, R. K. Thauer and G. L. Waldrop, *Chem. Rev.*, 2013, **113**, 6621–6658.

26 S. Srinivasan, R. Mosdale, P. Stevens and C. Yang, *Annu. Rev. Energy Environ.*, 1999, **24**, 281–328.

27 A. A. Gewirth and M. S. Thorum, *Inorg. Chem.*, 2010, **49**, 3557–3566.

28 M. G. Walter, E. L. Warren, J. R. McKone, S. W. Boettcher, Q. Mi, E. A. Santori and N. S. Lewis, *Chem. Rev.*, 2010, **110**, 6446–6473.

29 D. G. Nocera, *Acc. Chem. Res.*, 2012, **45**, 767–776.

30 J. R. Ran, J. Zhang, J. G. Yu, M. Jaroniec and S. Z. Qiao, *Chem. Soc. Rev.*, DOI: 10.1039/C1033CS60425J.

31 B. A. Pinaud, J. D. Benck, L. C. Seitz, A. J. Forman, Z. B. Chen, T. G. Deutsch, B. D. James, K. N. Baum, G. N. Baum, S. Ardo, H. L. Wang, E. Miller and T. F. Jaramillo, *Energy Environ. Sci.*, 2013, **6**, 1983–2002.

32 D. Pletcher, *J. Appl. Electrochem.*, 1984, **14**, 403–415.

33 P. C. K. Vesborg and T. F. Jaramillo, *RSC Adv.*, 2012, **2**, 7933–7947.

34 J. R. McKone, S. C. Marinescu, B. S. Brunschwig, J. R. Winkler and H. B. Gray, *Chem. Sci.*, 2014, **5**, 865–878.

35 C. Z. Zhu and S. J. Dong, *Nanoscale*, 2013, **5**, 1753–1767.

36 K. P. Gong, F. Du, Z. H. Xia, M. Durstock and L. M. Dai, *Science*, 2009, **323**, 760–764.

37 Y. W. Cheng, H. B. Zhang, C. V. Varanasi and J. Liu, *Sci. Rep.*, 2013, **3**, 3195.

38 A. Malinauskas, *Synth. Met.*, 1999, **107**, 75–83.

39 Z. W. Chen, D. Higgins, A. P. Yu, L. Zhang and J. J. Zhang, *Energy Environ. Sci.*, 2011, **4**, 3167–3192.

40 A. J. Esswein and D. G. Nocera, *Chem. Rev.*, 2007, **107**, 4022–4047.

41 V. Artero and M. Fontecave, *Coord. Chem. Rev.*, 2005, **249**, 1518–1535.

42 V. Artero, M. Chavarot-Kerlidou and M. Fontecave, *Angew. Chem. Int. Ed.*, 2011, **50**, 7238–7266.

43 J. L. Dempsey, B. S. Brunschwig, J. R. Winkler and H. B. Gray, *Acc. Chem. Res.*, 2009, **42**, 1995–2004.

44 P. W. Du and R. Eisenberg, *Energy Environ. Sci.*, 2012, **5**, 6012–6021.

45 C. Finn, S. Schnittger, L. J. Yellowlees and J. B. Love, *Chem. Commun.*, 2012, **48**, 1392–1399.

46 V. S. Thoi, Y. J. Sun, J. R. Long and C. J. Chang, *Chem. Soc. Rev.*, 2013, **42**, 2388–2400.

47 J. O. M. Bockris and E. C. Potter, *J. Electrochem. Soc.*, 1952, **99**, 169–186.

48 I. E. L. Stephens, A. S. Bondarenko, U. Grønbjerg, J. Rossmeisl and I. Chorkendorff, *Energy Environ. Sci.*, 2012, **5**, 6744–6762.

49 A. J. Bard and L. R. Faulkner, *Electrochemical Methods: Fundamentals and Applications*, Wiley, New York, 2001.

50 M. S. Faber, R. Dziedzic, M. A. Lukowski, N. S. Kaiser, Q. Ding and S. Jin, *J. Am. Chem. Soc.*, 2014, **136**, 10053–10061.

51 M. A. Lukowski, A. S. Daniel, C. R. English, F. Meng, A. Forticaux, R. J. Hamers and S. Jin, *Energy Environ. Sci.*, 2014, **7**, 2608–2613.

52 C. C. L. McCrory, S. H. Jung, J. C. Peters and T. F. Jaramillo, *J. Am. Chem. Soc.*, 2013, **135**, 16977–16987.

53 M. X. Wu and T. L. Ma, *ChemSusChem*, 2012, **5**, 1343–1357.

54 Y. Hou, D. Wang, X. H. Yang, W. Q. Fang, B. Zhang, H. F. Wang, G. Z. Lu, P. Hu, H. J. Zhao and H. G. Yang, *Nature Commun.*, 2013, **4**, DOI: 10.1038/Ncomms2547.

55 M. X. Wu and T. L. Ma, *J. Phys. Chem. C*, 2014, **118**, 16727–16742.

56 R. Parsons, *Trans. Faraday Soc.*, 1958, **54**, 1053–1063.

57 J. K. Nørskov, T. Bligaard, A. Logadottir, J. R. Kitchin, J. G. Chen, S. Pandelov and U. Stimming, *J. Electrochem. Soc.*, 2005, **152**, J23–J26.

58 J. K. Nørskov, J. Rossmeisl, A. Logadottir, L. Lindqvist, J. R. Kitchin, T. Bligaard and H. Jónsson, *J. Phys. Chem. B*, 2004, **108**, 17886–17892.

59 T. Weber, R. Prins and R. A. van Santen, eds., *Transition Metal Sulphides: Chemistry and Catalysis*, Kluwer Academic Publishers, Dordrecht, 1998.

60 A.-M. Alexander and J. S. J. Hargreaves, *Chem. Soc. Rev.*, 2010, **39**, 4388–4401.

61 R. R. Chianelli, G. Berhault, P. Raybaud, S. Kasztelan, J. Hafner and H. Toulhoat, *Appl. Catal. A*, 2002, **227**, 83–96.

62 S. D. Jackson and J. S. J. Hargreaves, eds., *Metal Oxide Catalysis*, Wiley-VCH, Weinheim, 2009.

63 R. P. F. Gregory, *Biochemistry of Photosynthesis*, Wiley-Interscience, New York, 1989.

64 E. S. Andreiadis, P. A. Jacques, P. D. Tran, A. Leyris, M. Chavarot-Kerlidou, B. Jousselme, M. Matheron, J. Pécaut, S. Palacin, M. Fontecave and V. Artero, *Nature Chem.*, 2013, **5**, 48–53.

65 T. F. Jaramillo, J. Bonde, J. D. Zhang, B.-L. Ooi, K. Andersson, J. Ulstrup and I. Chorkendorff, *J. Phys. Chem. C*, 2008, **112**, 17492–17498.

66 Y. D. Hou, B. L. Abrams, P. C. K. Vesborg, M. E. Björketun, K. Herbst, L. Bech, A. M. Setti, C. D. Damsgaard, T. Pedersen, O. Hansen, J. Rossmeisl, S. Dahl, J. K. Nørskov and I. Chorkendorff, *Nature Mater.*, 2011, **10**, 434–438.

67 G. Hodes, J. Manassen and D. Cahen, *J. Electrochem. Soc.*, 1980, **127**, 544–549.

68 S. Trasatti, *J. Electroanal. Chem.*, 1972, **39**, 163–184.

69 M. H. Miles, *J. Electroanal. Chem.*, 1975, **60**, 89–96.

70 A. T. Kuhn, C. J. Mortimer, G. C. Bond and J. Lindley, *J. Electroanal. Chem.*, 1972, **34**, 1–14.

71 J. G. Highfield, E. Claude and K. Oguro, *Electrochim. Acta*, 1999, **44**, 2805–2814.

72 M. M. Jaksic, *Int. J. Hydrogen Energy*, 2001, **26**, 559–578.

73 J. Greeley, J. K. Nørskov, L. A. Kibler, A. M. El-Aziz and D. M. Kolb, *ChemPhysChem*, 2006, **7**, 1032–1035.

74 J. Greeley, I. E. L. Stephens, A. S. Bondarenko, T. P. Johansson, H. A. Hansen, T. F. Jaramillo, J. Rossmeisl, I. Chorkendorff and J. K. Nørskov, *Nature Chem.*, 2009, **1**, 552–556.

75 E. W. Brooman and A. T. Kuhn, *J. Electroanal. Chem.*, 1974, **49**, 325–353.

76 D. E. Brown, M. N. Mahmood, A. K. Turner, S. M. Hall and P. O. Fogarty, *Int. J. Hydrogen Energy*, 1982, **7**, 405–410.

77 D. E. Brown, M. N. Mahmood, M. C. M. Man and A. K. Turner, *Electrochim. Acta*, 1984, **29**, 1551–1556.

78 E. Navarro-Flores, Z. W. Chong and S. Omanovic, *J. Mol. Catal. A: Chem.*, 2005, **226**, 179–197.

79 J. R. McKone, B. F. Sadtler, C. A. Werlang, N. S. Lewis and H. B. Gray, *ACS Catal.*, 2013, **3**, 166–169.

80 J. R. McKone, E. L. Warren, M. J. Bierman, S. W. Boettcher, B. S. Brunschwig, N. S. Lewis and H. B. Gray, *Energy Environ. Sci.*, 2011, **4**, 3573–3583.

81 E. L. Warren, J. R. McKone, H. A. Atwater, H. B. Gray and N. S. Lewis, *Energy Environ. Sci.*, 2012, **5**, 9653–9661.

82 B. E. Conway and L. Bai, *Int. J. Hydrogen Energy*, 1986, **11**, 533–540.

83 I. A. Raj, *Int. J. Hydrogen Energy*, 1992, **17**, 413–421.

84 S. Y. Reece, J. A. Hamel, K. Sung, T. D. Jarvi, A. J. Esswein, J. J. H. Pijpers and D. G. Nocera, *Science*, 2011, **334**, 645–648.

85 S. Trasatti, *Electrodes of Conductive Metallic Oxides*, Elsevier Scientific Pub. Co., 1980.

86 F. Y. Cheng, Y. Su, J. Liang, Z. L. Tao and J. Chen, *Chem. Mater.*, 2010, **22**, 898–905.

87 F. Y. Cheng, J. A. Shen, B. Peng, Y. D. Pan, Z. L. Tao and J. Chen, *Nature Chem.*, 2011, **3**, 79–84.

88 T. Maiyalagan, K. A. Jarvis, S. Therese, P. J. Ferreira and A. Manthiram, *Nature Commun.*, 2014, **5**, DOI: 10.1038/ncomms4949.

89 J. Suntivich, H. A. Gasteiger, N. Yabuuchi, H. Nakanishi, J. B. Goodenough and Y. Shao-Horn, *Nature Chem.*, 2011, **3**, 546–550.

90 Y. Y. Liang, Y. G. Li, H. L. Wang and H. J. Dai, *J. Am. Chem. Soc.*, 2013, **135**, 2013–2036.

91 Y. Y. Liang, Y. G. Li, H. L. Wang, J. G. Zhou, J. Wang, T. Regier and H. J. Dai, *Nature Mater.*, 2011, **10**, 780–786.

92 M.-R. Gao, S. A. Liu, J. Jiang, C.-H. Cui, W.-T. Yao and S.-H. Yu, *J. Mater. Chem.*, 2010, **20**, 9355–9361.

93 Y.-F. Xu, M.-R. Gao, Y.-R. Zheng, J. Jiang and S.-H. Yu, *Angew. Chem. Int. Ed.*, 2013, **52**, 8546–8550.

94 R. Ohnishi, Y. Takahashi, A. Takagaki, J. Kubota and K. Domen, *Chem. Lett.*, 2008, **37**, 838–839.

95 X. Lin, M. X. Wu, Y. D. Wang, A. Hagfeldt and T. L. Ma, *Chem. Commun.*, 2011, **47**, 11489–11491.

96 J. A. Wilson and A. D. Yoffe, *Adv. Phys.*, 1969, **18**, 193–335.

97 W. Jaegermann and H. Tributsch, *Prog. Surf. Sci.*, 1988, **29**, 1–167.

98 H. Gerischer, *J. Electroanal. Chem. Interfacial Electrochem.*, 1975, **58**, 263–274.

99 G. Hodes, J. Manassen and D. Cahen, *Nature*, 1976, **261**, 403–404.

100 B. Miller and A. Heller, *Nature*, 1976, **262**, 680–681.

101 A. B. Ellis, S. W. Kaiser and M. S. Wrighton, *J. Am. Chem. Soc.*, 1976, **98**, 1635–1637.

102 P. L. Allen and A. Hickling, *Trans. Faraday Soc.*, 1957, **53**, 1626–1635.

103 T. Loučka, *J. Electroanal. Chem.*, 1972, **36**, 369–381.

104 J. G. Radich, R. Dwyer and P. V. Kamat, *J. Phys. Chem. Lett.*, 2011, **2**, 2453–2460.

105 J. G. Radich, N. R. Peeples, P. K. Santra and P. V. Kamat, *J. Phys. Chem. C*, 2014, **118**, 16463–16471.

106 M. Chhowalla, H. S. Shin, G. Eda, L.-J. Li, K. P. Loh and H. Zhang, *Nature Chem.*, 2013, **5**, 263–275.

107 J. Yang and H. S. Shin, *J. Mater. Chem. A*, 2014, **2**, 5979–5985.

108 D. Merki and X. L. Hu, *Energy Environ. Sci.*, 2011, **4**, 3878–3888.

109 A. B. Laursen, S. Kegnæs, S. Dahl and I. Chorkendorff, *Energy Environ. Sci.*, 2012, **5**, 5577–5591.

110 B. Hinnemann, P. G. Moses, J. Bonde, K. P. Jørgensen, J. H. Nielsen, S. Horch, I. Chorkendorff and J. K. Nørskov, *J. Am. Chem. Soc.*, 2005, **127**, 5308–5309.

111 T. F. Jaramillo, K. P. Jørgensen, J. Bonde, J. H. Nielsen, S. Horch and I. Chorkendorff, *Science*, 2007, **317**, 100–102.

112 J. Bonde, P. G. Moses, T. F. Jaramillo, J. K. Nørskov and I. Chorkendorff, *Faraday Discuss.*, 2008, **140**, 219–231.

113 H. I. Karunadasa, E. Montalvo, Y. J. Sun, M. Majda, J. R. Long and C. J. Chang, *Science*, 2012, **335**, 698–702.

114 R. Tenne and M. Redlich, *Chem. Soc. Rev.*, 2010, **39**, 1423–1434.

115 Y. G. Li, H. L. Wang, L. M. Xie, Y. Y. Liang, G. S. Hong and H. J. Dai, *J. Am. Chem. Soc.*, 2011, **133**, 7296–7299.

116 M. A. Lukowski, A. S. Daniel, F. Meng, A. Forticaux, L. Li and S. Jin, *J. Am. Chem. Soc.*, 2013, **135**, 10274–10277.

117 D. Voiry, H. Yamaguchi, J. Li, R. Silva, D. C. B. Alves, T. Fujita, M. Chen, T. Asefa, V. B. Shenoy, G. Eda and M. Chhowalla, *Nature Mater.*, 2013, **12**, 850–855.

118 D. S. Kong, H. T. Wang, J. J. Cha, M. Pasta, K. J. Koski, J. Yao and Y. Cui, *Nano Lett.*, 2013, **13**, 1341–1347.

119 H. Wang, Z. Lu, S. Xu, D. Kong, J. J. Cha, G. Zheng, P.-C. Hsu, K. Yan, D. Bradshaw, F. B. Prinz and Y. Cui, *Proc. Natl. Acad. Sci. U.S.A.*, 2013, **110**, 19701–19706.

120 J. F. Xie, H. Zhang, S. Li, R. X. Wang, X. Sun, M. Zhou, J. F. Zhou, X. W. Lou and Y. Xie, *Adv. Mater.*, 2013, **25**, 5807–5813.

121 J. F. Xie, J. J. Zhang, S. Li, F. Grote, X. D. Zhang, H. Zhang, R. X. Wang, Y. Lei, B. C. Pan and Y. Xie, *J. Am. Chem. Soc.*, 2013, **135**, 17881–17888.

122 D. Y. Chung, S.-K. Park, Y.-H. Chung, S.-H. Yu, D.-H. Lim, N. Jung, H. C. Ham, H.-Y. Park, Y. Piao, S. J. Yoo and Y.-E. Sung, *Nanoscale*, 2014, **6**, 2131–2136.

123 X. L. Zheng, J. B. Xu, K. Y. Yan, H. Wang, Z. L. Wang and S. H. Yang, *Chem. Mater.*, 2014, **26**, 2344–2353.

124 Z. Y. Lu, W. Zhu, X. Y. Yu, H. C. Zhang, Y. J. Li, X. M. Sun, X. W. Wang, H. Wang, J. M. Wang, J. Luo, X. D. Lei and L. Jiang, *Adv. Mater.*, 2014, **26**, 2683–2687.

125 J. Kibsgaard, Z. Chen, B. N. Reinecke and T. F. Jaramillo, *Nature Mater.*, 2012, **11**, 963–969.

126 D. Z. Wang, Z. P. Wang, C. L. Wang, P. Zhou, Z. Z. Wu and Z. H. Liu, *Electrochem. Commun.*, 2013, **34**, 219–222.

127 Q. Ding, F. Meng, C. R. English, M. Cabán-Acevedo, M. J. Shearer, D. Liang, A. S. Daniel, R. J. Hamers and S. Jin, *J. Am. Chem. Soc.*, 2014, **136**, 8504–8507.

128 Z. Z. Wu, B. Z. Fang, A. Bonakdarpour, A. K. Sun, D. P. Wilkinson and D. Z. Wang, *Appl. Catal. B*, 2012, **125**, 59–66.

129 J. Lin, Z. W. Peng, G. Wang, D. Zakhidov, E. Larios, M. J. Yacaman and J. M. Tour, *Adv. Energy Mater.*, DOI: 10.1002/aenm.201301875.

130 H. T. Wang, D. S. Kong, P. Johanes, J. J. Cha, G. Y. Zheng, K. Yan, N. A. Liu and Y. Cui, *Nano Lett.*, 2013, **13**, 3426–3433.

131 C.-H. Lai, M.-Y. Lu and L.-J. Chen, *J. Mater. Chem.*, 2012, **22**, 19–30.

132 M.-R. Gao, Y.-F. Xu, J. Jiang and S.-H. Yu, *Chem. Soc. Rev.*, 2013, **42**, 2986–3017.

133 X. Huang, Z. Y. Zeng and H. Zhang, *Chem. Soc. Rev.*, 2013, **42**, 1934–1946.

134 C. G. Morales-Guio, L.-A. Stern and X. L. Hu, *Chem. Soc. Rev.*, DOI: 10.1039/C1033CS60468C.

135 J. H. Guo, Y. T. Shi, C. Zhu, L. Wang, N. Wang and T. L. Ma, *J. Mater. Chem. A*, 2013, **1**, 11874–11879.

136 I. A. Ji, H. M. Choi and J. H. Bang, *Mater. Lett.*, 2014, **123**, 51–54.

137 S. T. Finn and J. E. Macdonald, *Adv. Energy Mater.*, 2014, DOI: 10.1002/aenm.201400495.

138 M. S. Faber, K. Park, M. Cabán-Acevedo, P. K. Santra and S. Jin, *J. Phys. Chem. Lett.*, 2013, **4**, 1843–1849.

139 M. S. Faber, M. A. Lukowski, Q. Ding, N. S. Kaiser and S. Jin, *J. Phys. Chem. C*, 2014, in press.

140 X. L. Duan, Z. Y. Gao, J. L. Chang, D. P. Wu, P. F. Ma, J. J. He, F. Xu, S. Y. Gao and K. Jiang, *Electrochim. Acta*, 2013, **114**, 173–179.

141 Q.-H. Huang, T. Ling, S.-Z. Qiao and X.-W. Du, *J. Mater. Chem. A*, 2013, **1**, 11828–11833.

142 Y.-C. Wang, D.-Y. Wang, Y.-T. Jiang, H.-A. Chen, C.-C. Chen, K.-C. Ho, H.-L. Chou and C.-W. Chen, *Angew. Chem. Int. Ed.*, 2013, **52**, 6694–6698.

143 M. Cabán-Acevedo, M. S. Faber, Y. Z. Tan, R. J. Hamers and S. Jin, *Nano Lett.*, 2012, **12**, 1977–1982.

144 M. Cabán-Acevedo, D. Liang, K. S. Chew, J. P. DeGrave, N. S. Kaiser and S. Jin, *ACS Nano*, 2013, **7**, 1731–1739.

145 S. J. Peng, L. L. Li, H. T. Tan, R. Cai, W. H. Shi, C. C. Li, S. G. Mhaisalkar, M. Srinivasan, S. Ramakrishna and Q. Y. Yan, *Adv. Funct. Mater.*, 2014, **24**, 2155–2162.

146 D. Baresel, W. Sarholz, P. Scharner and J. Schmitz, *Berich. Bunsen Gesell.*, 1974, **78**, 608–611.

147 D. Susac, L. Zhu, M. Teo, A. Sode, K. C. Wong, P. C. Wong, R. R. Parsons, D. Bizzotto, K. A. R. Mitchell and S. A. Campbell, *J. Phys. Chem. C*, 2007, **111**, 18715–18723.

148 L. Zhu, D. Susac, M. Teo, K. C. Wong, P. C. Wong, R. R. Parsons, D. Bizzotto, K. A. R. Mitchell and S. A. Campbell, *J. Catal.*, 2008, **258**, 235–242.

149 L. Zhu, M. Teo, P. C. Wong, K. C. Wong, I. Narita, F. Ernst, K. A. R. Mitchell and S. A. Campbell, *Appl. Catal. A*, 2010, **386**, 157–165.

150 J. S. Jirkovský, A. Björling and E. Ahlberg, *J. Phys. Chem. C*, 2012, **116**, 24436–24444.

151 C. Zhao, D. Li and Y. Feng, *J. Mater. Chem. A*, 2013, **1**, 5741–5746.

152 J. Kibsgaard, T. F. Jaramillo and F. Besenbacher, *Nature Chem.*, 2014, **6**, 248–253.

153 A. Ivanovskaya, N. Singh, R.-F. Liu, H. Kreutzer, J. Baltrusaitis, T. V. Nguyen, H. Metiu and E. McFarland, *Langmuir*, 2013, **29**, 480–492.

154 D. S. Kong, H. T. Wang, Z. Y. Lu and Y. Cui, *J. Am. Chem. Soc.*, 2014, **136**, 4897–4900.

155 D. S. Kong, J. J. Cha, H. T. Wang, H. R. Lee and Y. Cui, *Energy Environ. Sci.*, 2013, **6**, 3553–3558.

156 D. Merki, S. Fierro, H. Vrubel and X. L. Hu, *Chem. Sci.*, 2011, **2**, 1262–1267.

157 B. Seger, A. B. Laursen, P. C. K. Vesborg, T. Pedersen, O. Hansen, S. Dahl and I. Chorkendorff, *Angew. Chem. Int. Ed.*, 2012, **51**, 9128–9131.

158 T. Y. Wang, J. Q. Zhuo, K. Z. Du, B. B. Chen, Z. W. Zhu, Y. H. Shao and M. X. Li, *Adv. Mater.*, DOI: 10.1002/adma.201400265.

159 C. G. Morales-Guio, S. D. Tilley, H. Vrubel, M. Grätzel and X. L. Hu, *Nature Commun.*, 2014, **5**, DOI: 10.1038/ncomms4059.

160 J. D. Benck, Z. B. Chen, L. Y. Kuritzky, A. J. Forman and T. F. Jaramillo, *ACS Catal.*, 2012, **2**, 1916–1923.

161 H. Vrubel, D. Merki and X. L. Hu, *Energy Environ. Sci.*, 2012, **5**, 6136–6144.

162 D. J. Li, U. N. Maiti, J. Lim, D. S. Choi, W. J. Lee, Y. Oh, G. Y. Lee and S. O. Kim, *Nano Lett.*, 2014, **14**, 1228–1233.

163 Y.-H. Chang, C.-T. Lin, T.-Y. Chen, C.-L. Hsu, Y.-H. Lee, W. J. Zhang, K.-H. Wei and L.-J. Li, *Adv. Mater.*, 2013, **25**, 756–760.

164 X. Zong, H. J. Yan, G. P. Wu, G. J. Ma, F. Y. Wen, L. Wang and C. Li, *J. Am. Chem. Soc.*, 2008, **130**, 7176–7177.

165 A. B. Laursen, T. Pedersen, P. Malacrida, B. Seger, O. Hansen, P. C. K. Vesborg and I. Chorkendorff, *Phys. Chem. Chem. Phys.*, 2013, **15**, 20000–20004.

166 Y. Sun, C. Liu, D. C. Grauer, J. Yano, J. R. Long, P. Yang and C. J. Chang, *J. Am. Chem. Soc.*, 2013, **135**, 17699–17702.

167 M.-R. Gao, Z.-Y. Lin, T.-T. Zhuang, J. Jiang, Y.-F. Xu, Y.-R. Zheng and S.-H. Yu, *J. Mater. Chem.*, 2012, **22**, 13662–13668.

168 M. K. Wang, A. M. Anghel, B. Marsan, N.-L. C. Ha, N. Pootrakulchote, S. M. Zakeeruddin and M. Grätzel, *J. Am. Chem. Soc.*, 2009, **131**, 15976–15977.

169 C.-W. Kung, H.-W. Chen, C.-Y. Lin, K.-C. Huang, R. Vittal and K.-C. Ho, *ACS Nano*, 2012, **6**, 7016–7025.

170 S.-H. Chang, M.-D. Lu, Y.-L. Tung and H.-Y. Tuan, *ACS Nano*, 2013, **7**, 9443–9451.

171 H. C. Sun, D. Qin, S. Q. Huang, X. Z. Guo, D. M. Li, Y. H. Luo and Q. B. Meng, *Energy Environ. Sci.*, 2011, **4**, 2630–2637.

172 H. M. Choi, I. A. Ji and J. H. Bang, *ACS Appl. Mater. Interfaces*, 2014, **6**, 2335–2343.

173 F. Gong, H. Wang, X. Xu, G. Zhou and Z.-S. Wang, *J. Am. Chem. Soc.*, 2012, **134**, 10953–10958.

174 J. G. G. Chen, *Chem. Rev.*, 1996, **96**, 1477–1498.

175 W.-F. Chen, J. T. Muckerman and E. Fujita, *Chem. Commun.*, 2013, **49**, 8896–8909.

176 W.-F. Chen, K. Sasaki, C. Ma, A. I. Frenkel, N. Marinkovic, J. T. Muckerman, Y. M. Zhu and R. R. Adzic, *Angew. Chem. Int. Ed.*, 2012, **51**, 6131–6135.

177 B. F. Cao, G. M. Veith, J. C. Neuefeind, R. R. Adzic and P. G. Khalifah, *J. Am. Chem. Soc.*, 2013, **135**, 19186–19192.

178 M. J. Liu, Y. Z. Dong, Y. M. Wu, H. B. Feng and J. H. Li, *Chem. Eur. J.*, 2013, **19**, 14781–14786.

179 G. R. Li, J. Song, G. L. Pan and X. P. Gao, *Energy Environ. Sci.*, 2011, **4**, 1680–1683.

180 X. Y. Zhang, X. Chen, K. J. Zhang, S. P. Pang, X. H. Zhou, H. X. Xu, S. M. Dong, P. X. Han, Z. Y. Zhang, C. J. Zhang and G. L. Cui, *J. Mater. Chem. A*, 2013, **1**, 3340–3346.

181 G.-R. Li, F. Wang, Q.-W. Jiang, X.-P. Gao and P.-W. Shen, *Angew. Chem. Int. Ed.*, 2010, **49**, 3653–3656.

182 N. P. Sweeny, C. S. Rohrer and O. W. Brown, *J. Am. Chem. Soc.*, 1958, **80**, 799–800.

183 S. T. Oyama, *J. Catal.*, 2003, **216**, 343–352.

184 S. T. Oyama, T. Gott, H. Y. Zhao and Y.-K. Lee, *Catal Today*, 2009, **143**, 94–107.

185 S. Carenco, D. Portehault, C. Boissière, N. Mézailles and C. Sanchez, *Chem. Rev.*, 2013, **113**, 7981–8065.

186 I. Paseka, *Electrochim. Acta*, 1995, **40**, 1633–1640.

187 J.-F. Deng, H. X. Li and W. J. Wang, *Catal Today*, 1999, **51**, 113–125.

188 Y. Xu, R. Wu, J. F. Zhang, Y. M. Shi and B. Zhang, *Chem. Commun.*, 2013, **49**, 6656–6658.

189 E. J. Popczun, J. R. McKone, C. G. Read, A. J. Biacchi, A. M. Wiltrout, N. S. Lewis and R. E. Schaak, *J. Am. Chem. Soc.*, 2013, **135**, 9267–9270.

190 E. J. Popczun, C. G. Read, C. W. Roske, N. S. Lewis and R. E. Schaak, *Angew. Chem. Int. Ed.*, 2014, **53**, 5427–5430.

191 J. Q. Tian, Q. Liu, A. M. Asiri and X. P. Sun, *J. Am. Chem. Soc.*, 2014, **136**, 7587–7590.

192 Z. H. Pu, Q. Liu, P. Jiang, A. M. Asiri, A. Y. Obaid and X. P. Sun, *Chem. Mater.*, 2014, DOI: 10.1021/cm501273s.

193 Q. Liu, J. Q. Tian, W. Cui, P. Jiang, N. Y. Cheng, A. M. Asiri and X. P. Sun, *Angew. Chem. Int. Ed.*, 2014, **53**, 6710–6714.

194 P. Xiao, M. A. Sk, L. Thia, X. M. Ge, R. J. Lim, J.-Y. Wang, K. H. Lim and X. Wang, *Energy Environ. Sci.*, 2014, **7**, 2624–2629.

195 Y. Y. Dou, G. R. Li, J. Song and X. P. Gao, *Phys. Chem. Chem. Phys.*, 2012, **14**, 1339–1342.

196 M. X. Wu, J. Bai, Y. D. Wang, A. J. Wang, X. Lin, L. Wang, Y. H. Shen, Z. Q. Wang, A. Hagfeldt and T. L. Ma, *J. Mater. Chem.*, 2012, **22**, 11121–11127.

197 R. B. Levy and M. Boudart, *Science*, 1973, **181**, 547–549.

198 S. T. Oyama, ed., *The Chemistry of Transition Metal Carbides and Nitrides*, Chapman & Hall, London, 1996.

199 H. H. Hwu and J. G. G. Chen, *Chem. Rev.*, 2005, **105**, 185–212.

200 M. C. Weidman, D. V. Esposito, Y.-C. Hsu and J. G. G. Chen, *J. Power Sources*, 2012, **202**, 11–17.

201 H. Vrubel and X. L. Hu, *Angew. Chem. Int. Ed.*, 2012, **51**, 12703–12706.

202 L. Liao, S. N. Wang, J. J. Xiao, X. J. Bian, Y. H. Zhang, M. D. Scanlon, X. L. Hu, Y. Tang, B. H. Liu and H. H. Girault, *Energy Environ. Sci.*, 2014, **7**, 387–392.

203 P. Xiao, Y. Yan, X. M. Ge, Z. L. Liu, J.-Y. Wang and X. Wang, *Appl. Catal. B*, 2014, **154–155**, 232–237.

204 W.-F. Chen, C.-H. Wang, K. Sasaki, N. Marinkovic, W. Xu, J. T. Muckerman, Y. Zhu and R. R. Adzic, *Energy Environ. Sci.*, 2013, **6**, 943–951.

205 C. Wan, Y. N. Regmi and B. M. Leonard, *Angew. Chem. Int. Ed.*, DOI: 10.1002/anie.201402998.

206 S. P. Berglund, H. C. He, W. D. Chemelewski, H. Celio, A. Dolocan and C. B. Mullins, *J. Am. Chem. Soc.*, 2014, **136**, 1535–1544.

207 M. X. Wu, X. A. Lin, A. Hagfeldt and T. L. Ma, *Angew. Chem. Int. Ed.*, 2011, **50**, 3520–3524.

208 J. S. Jang, D. J. Ham, E. Ramasamy, J. Lee and J. S. Lee, *Chem. Commun.*, 2010, **46**, 8600–8602.

209 W. Guo, Y. H. Shen, M. X. Wu, L. Wang, L. L. Wang and T. L. Ma, *Chem. Eur. J.*, 2012, **18**, 7862–7868.

210 M.-H. Yeh, L.-Y. Lin, C.-P. Lee, C.-Y. Chou, K.-W. Tsai, J.-T. Lin and K.-C. Ho, *J. Power Sources*, 2013, **237**, 141–148.

211 A. W. Searcy, in *Chemical and mechanical behavior of inorganic materials*, eds. A. W. Searcy, D. V. Ragone and U. Colombo, Wiley-Interscience, New York, 1970.

212 X. Chen, X. K. Wang, J. H. Xiu, C. T. Williams and C. H. Liang, *J. Phys. Chem. C*, 2012, **116**, 24968–24976.

213 X. Chen, X. Liu, L. Wang, M. Li, C. T. Williams and C. H. Liang, *RSC Adv.*, 2013, **3**, 1728–1731.

214 X. Chen, J. H. Jin, G. Y. Sha, C. Li, B. S. Zhang, D. S. Su, C. T. Williams and C. H. Liang, *Catal. Sci. Technol.*, 2014, **4**, 53–61.

215 A. K. Vijh, G. Bélanger and R. Jacques, *Int. J. Hydrogen Energy*, 1990, **15**, 789–794.

216 A. K. Vijh, G. Bélanger and R. Jacques, *Int. J. Hydrogen Energy*, 1992, **17**, 479–483.

217 A. K. Vijh and G. Bélanger, *J. Mater. Sci. Lett.*, 1995, **14**, 982–984.

218 S. Wirth, F. Harnisch, M. Weinmann and U. Schröder, *Appl. Catal. B*, 2012, **126**, 225–230.

219 A. L. Schmitt, J. M. Higgins, J. R. Szczech and S. Jin, *J. Mater. Chem.*, 2010, **20**, 223–235.

220 M. Estruga, S. N. Girard, Q. Ding, L. Y. Chen, X. C. Li and S. Jin, *Chem. Commun.*, 2014, **50**, 1454–1457.

221 J. R. Szczech and S. Jin, *J. Mater. Chem.*, 2010, **20**, 1375–1382.

222 P. Los and A. Lasia, *J. Electroanal. Chem.*, 1992, **333**, 115–125.

223 J. J. Borodzínski and A. Lasia, *J. Appl. Electrochem.*, 1994, **24**, 1267–1275.

224 G. Wu, K. L. More, C. M. Johnston and P. Zelenay, *Science*, 2011, **332**, 443–447.

225 Y. Zhao, K. Kamiya, K. Hashimoto and S. Nakanishi, *Angew. Chem. Int. Ed.*, 2013, **52**, 13638–13641.

226 M. J. Bierman and S. Jin, *Energy Environ. Sci.*, 2009, **2**, 1050–1059.

227 F. Meng, S. A. Morin, A. Forticaux and S. Jin, *Acc. Chem. Res.*, 2013, **46**, 1616–1626.

228 M. A. Py and R. R. Haering, *Can J Phys*, 1983, **61**, 76–84.

229 C. Tsai, F. Abild-Pedersen and J. K. Nørskov, *Nano Lett.*, 2014, **14**, 1381–1387.

230 Y. Yan, B. Y. Xia, X. Y. Qi, H. B. Wang, R. Xu, J.-Y. Wang, H. Zhang and X. Wang, *Chem. Commun.*, 2013, **49**, 4884–4886.

231 W.-F. Chen, S. Iyer, S. Iyer, K. Sasaki, C.-H. Wang, Y. M. Zhu, J. T. Muckerman and E. Fujita, *Energy Environ. Sci.*, 2013, **6**, 1818–1826.

232 M. Woodhouse and B. A. Parkinson, *Chem. Soc. Rev.*, 2009, **38**, 197–210.

233 J. E. Katz, T. R. Gingrich, E. A. Santori and N. S. Lewis, *Energy Environ. Sci.*, 2009, **2**, 103–112.

234 C. X. Xiang, S. K. Suram, J. A. Haber, D. W. Guevarra, E. Soedarmadji, J. Jin and J. M. Gregoire, *ACS Comb. Sci.*, 2014, **16**, 47–52.

235 J. B. Gerken, S. E. Shaner, R. C. Massé, N. J. Porubsky and S. S. Stahl, *Energy Environ. Sci.*, 2014, **7**, 2376–2382.